Atmos. Chem. Phys., 21, 15519–15554, 2021
https://doi.org/10.5194/acp-21-15519-2021

Atmospheric Chemistry and Physics
Open Access
EGU

Twenty years of ground-based NDACC FTIR spectrometry at Izaña Observatory – overview and long-term comparison to other techniques

Omaira E. García[1], Matthias Schneider[2], Eliezer Sepúlveda[1], Frank Hase[2], Thomas Blumenstock[2], Emilio Cuevas[1], Ramón Ramos[1], Jochen Gross[2], Sabine Barthlott[2], Amelie N. Röhling[2], Esther Sanromá[1,a], Yenny González[1,3], Ángel J. Gómez-Peláez[1,b], Mónica Navarro-Comas[4], Olga Puentedura[4], Margarita Yela[4], Alberto Redondas[1], Virgilio Carreño[1], Sergio F. León-Luis[1,c], Enrique Reyes[1], Rosa D. García[1,5,c], Pedro P. Rivas[1], Pedro M. Romero-Campos[1], Carlos Torres[1], Natalia Prats[1], Miguel Hernández[6], and César López[7]

[1]Izaña Atmospheric Research Centre (IARC), State Meteorological Agency of Spain (AEMet), Santa Cruz de Tenerife, Spain
[2]Karlsruhe Institute of Technology (KIT), Institute of Meteorology and Climate Research (IMK-ASF), Karlsruhe, Germany
[3]Cimel Electronique, Paris, France
[4]Atmospheric Research and Instrumentation Branch, National Institute for Aerospace Technology (INTA), Madrid, Spain
[5]Group of Atmospheric Optic, University of Valladolid, Valladolid, Spain
[6]Canarias Delegation, State Meteorological Agency of Spain (AEMet), Santa Cruz de Tenerife, Spain
[7]Sieltec Canarias S.L., La Laguna, Spain
[a]now at: Employment Observatory of the Canary Islands (OBECAN), Santa Cruz de Tenerife, Spain
[b]now at: Asturias Delegation, State Meteorological Agency of Spain (AEMet), Oviedo, Spain
[c]now at: TRAGSATEC, Madrid, Spain

Correspondence: Omaira E. García (ogarciar@aemet.es)

Received: 8 April 2021 – Discussion started: 31 May 2021
Revised: 8 September 2021 – Accepted: 22 September 2021 – Published: 18 October 2021

Abstract. High-resolution Fourier transform infrared (FTIR) solar observations are particularly relevant for climate studies, as they allow atmospheric gaseous composition and multiple climate processes to be monitored in detail. In this context, the present paper provides an overview of 20 years of FTIR measurements taken in the framework of the NDACC (Network for the Detection of Atmospheric Composition Change) from 1999 to 2018 at the subtropical Izaña Observatory (IZO, Spain). Firstly, long-term instrumental performance is comprehensively assessed, corroborating the temporal stability and reliable instrumental characterization of the two FTIR spectrometers installed at IZO since 1999. Then, the time series of all trace gases contributing to NDACC at IZO are presented (i.e. C_2H_6, CH_4, $ClONO_2$, CO, HCl, HCN, H_2CO, HF, HNO_3, N_2O, NO_2, NO, O_3, carbonyl sulfide (OCS), and water vapour isotopologues $H_2^{16}O$, $H_2^{18}O$, and $HD^{16}O$), reviewing the major accomplishments drawn from these observations. In order to examine the quality and long-term consistency of the IZO FTIR observations, a comparison of those NDACC products for which other high-quality measurement techniques are available at IZO has been performed (i.e. CH_4, CO, H_2O, NO_2, N_2O, and O_3). This quality assessment was carried out on different timescales to examine what temporal signals are captured by the FTIR records, and to what extent. After 20 years of operation, the IZO NDACC FTIR observations have been found to be very consistent and reliable over time, demonstrating great potential for climate research. Long-term NDACC FTIR data sets, such as IZO, are indispensable tools for the investigation of atmospheric composition trends, multi-year phenomena, and complex climate feedback processes, as well as for the validation of past and present space-based missions and chemistry climate models.

Published by Copernicus Publications on behalf of the European Geosciences Union.

1 Introduction

The recognition that changes in the composition of the Earth's atmosphere are occurring, on both long and short timescales and thereby modifying our environment and climate, has resulted in scientific debate, as well as public concern in the last decades (Gottwald et al., 2006). Established examples, such as depletion of the ozone layer, warming of air and oceans, rising sea level, or melting cryosphere, have widely been reported in literature (WMO, 2018; Masson-Delmotte et al., 2021, and references therein). In order to assess the significance of such changes and to better understand the physical and chemical processes involved, continuous, consistent, long-term monitoring of the atmospheric composition is indispensable. These observational data sets are also fundamental to testing the ability of current climate models to provide reliable projections of future climate, and thus, they are the basis for design and implementation of efficient climate-change mitigation and adaptation policies.

Among different atmospheric monitoring measurement techniques, Fourier transform infrared (FTIR) spectrometry is of particular interest for climate research. With this technique, the source radiation (typically the sun for atmospheric ground-based measurements) is modulated by an interferometer, and all optical frequencies are recorded simultaneously in the measured interferogram (Griffiths and de Haseth, 2007). Then, a mathematical Fourier transform is used to retrieve the atmospheric absorption spectrum from the interferogram. By analysing the pressure broadening effect on these measured solar spectra through inversion schemes, the FTIR technique can provide atmospheric concentrations of many different trace gases simultaneously (e.g. Hase et al., 2004; Schneider et al., 2005; Wunch et al., 2011; Schneider et al., 2012; Kohlhepp et al., 2012; García et al., 2012; Sepúlveda et al., 2014; Barthlott et al., 2015; Wunch et al., 2015; Vigouroux et al., 2018; De Mazière et al., 2018).

The first continuous or semi-continuous records of ground-based FTIR spectrometers started in the late 1970s and early 1980s in just a few stations around the world. Today, high-resolution FTIR instruments mainly operate at a global scale in the framework of two international networks for atmospheric composition monitoring: NDACC (Network for the Detection of Atmospheric Composition Change, https://www.ndaccdemo.org, last access: 1 April 2021) and TCCON (Total Carbon Column Observing Network, https://tccon-wiki.caltech.edu, last access: 1 April 2021). While NDACC aims mainly to establish a long-term database to detect changes and trends in atmospheric composition and to understand their impact on the Earth's atmosphere (De Mazière et al., 2018), TCCON focuses more on research on greenhouse gases, improving our understanding of the carbon cycle and providing reference validation data sets for climate models and space-based observations (Wunch et al., 2011). Recently, these high-resolution FTIR observations have been extended by COCCON (COllaborative Carbon Column Observing Network, Frey et al., 2019), a research infrastructure of portable, compact, low-resolution, ground-based FTIR instruments set up as a supplement to TCCON.

Given its strategic location, one of the most relevant ground-based FTIR stations is Izaña Observatory (IZO), where FTIR observations have been carried out since 1999 coincidentally with other high-quality atmospheric measurements (Cuevas et al., 2019). IZO is located in the subtropical belt ($\sim 30^\circ$ N), in the descending branch of the northern Hadley atmospheric circulation cell and within the so-called subtropical transport barrier (Schneider et al., 2005, and references therein). This area, the transition between tropics and mid-latitudes, plays a crucial role in the chemical and dynamical transport processes in the atmosphere and is a direct tracer of climate change. Recent studies have demonstrated, for example, that the tropical belt has expanded over the past few decades, meaning that the descending limb of the Hadley cells is shifting towards the poles in both hemispheres (Heffernan, 2016, and references therein). This poleward movement of large-scale atmospheric circulation systems, such as storm tracks and jet streams, and their associated subtropical dry zones, may lead to profound changes in the global climate system, affecting natural ecosystems, biodiversity, and water resources (Seidel et al., 2008). Together with the so-called tropical bloating, climate models predict a speed-up in the stratospheric Brewer–Dobson circulation in response to current global warming, boosting an ozone recovery in the extratropics at the expense of a delay in the tropics and subtropics (Hegglin and Shepherd, 2009; WMO, 2018; Masson-Delmotte et al., 2021, and references therein). Nevertheless, these complex phenomena and their implications for the Earth's climate system and, in particular, for tropical and subtropical regions, are still poorly understood (Seidel et al., 2008; Heffernan, 2016). Unfortunately, due mainly to geographical and political factors, these areas suffer from a great lack of observations that allow their atmospheric structure and composition to be comprehensively investigated. Hence, the high-quality long-term FTIR measurements acquired at IZO provide excellent potential for climate research.

In this context, the present paper gives an overview of the FTIR measurement programme at IZO, going over its history during its first 20 years of operation (1999–2018) and its current status, as well as exploring its great value for long-term climate research. Although the IZO FTIR station currently operates in the framework of NDACC, TCCON, and COCCON, this review work focuses on NDACC FTIR activities throughout the entire 20-year period. For this purpose, the current paper has been structured as follows: Sects. 2 and 3 describe the measurement site and NDACC FTIR products (solar measurements, retrieval principles and strategies, and product characterization), respectively. Section 4 assesses the long-term performance of the IZO FTIR instruments. Sections 5 and 6 present the time series of all products contributing to NDACC (total column – TC – amounts and volume

mixing ratio – VMR – vertical profiles), illustrating the potential of the long-term IZO records with some research examples, while Sect. 7 briefly reviews other scientific applications of the IZO NDACC data. In Sect. 8, quality assessment of the different NDACC products is carried out by comparing them to other high-quality measurement techniques available at IZO. Finally, Sect. 9 summarizes the most significant results and conclusions drawn from this work.

2 Izaña Observatory and FTIR programme

IZO is a high-mountain station located on the island of Tenerife (Canary Islands, Spain) in the subtropical North Atlantic Ocean (28.3° N, 16.5° W) at an altitude of 2.37 km a.s.l. (Fig. 1). The observatory is managed by the Izaña Atmospheric Research Centre (IARC, https://izana.aemet.es/, last access: 1 April 2021), which belongs to the State Meteorological Agency of Spain (AEMet).

IZO is located on the top plateau of Izaña mountain, normally above a well-established thermal inversion layer, and is characterized by the quasi-permanent subsidence regime typical for subtropical regions (Fig. 1b). Locally, diurnal insolation generates a slight up-slope flow of air originating from below the inversion layer that can disturb the free troposphere conditions at IZO. But, during night-time, the subsidence regime prevails, and the atmospheric observations taken at IZO are well-representative of the subtropical North Atlantic free troposphere (Cuevas et al., 2019, and references therein). This, together with the fact that IZO is far from principal pollutant emission sources, means there are very clean, dry atmospheric conditions at the observatory during most of the year. These environmental conditions account for the historical importance of this observatory and its comprehensive measurement programme for atmospheric composition monitoring. IZO was inaugurated in its present location on 1 January 1916, initiating uninterrupted meteorological and climatological observations until the present day (Cuevas et al., 2019). Since 1984, IZO has contributed to the GAW-WMO (Global Atmospheric Watch, World Meteorological Organization) programme and to multiple international networks and databases (WDCGG, WOUDC, NDACC, TCCON, AERONET, BSRN, MPLNET, E-GVAP, NOAA/ESRL/GMD CCGG, etc.). Refer to Cuevas et al. (2019) for more details about IZO and its atmospheric monitoring programmes.

Within IZO's atmospheric research activities, the FTIR programme was established in 1999, in the framework of a collaboration between the AEMet and the KIT (Karlsruhe Institute of Technology), with the main goals being the long-term monitoring of atmospheric gas composition and the validation of satellite remote sensing measurements and climate models (Schneider et al., 2005). Since then, two Bruker high-resolution FTIR systems have been operated at IZO: an IFS 120M from 1999 to 2005 and an IFS 120HR (upgraded to the 125HR model, so-called 120/5HR) from 2005 until present day. These activities have routinely contributed to NDACC and TCCON since 1999 and 2007, respectively. Since 2018 NDACC and TCCON activities have been complemented by a portable, low-resolution FTIR spectrometer (a Bruker EM27/SUN), which operates within the COCCON research infrastructure.

3 NDACC FTIR products

3.1 Solar measurements

The IZO FTIR instrument records direct solar absorption spectra in the near- and mid-infrared spectral region (NIR and MIR, respectively), using a set of different field stops, narrow-bandpass filters, and detectors. Within the NDACC activities, the solar spectra were acquired between 700 and 4500 cm^{-1} with a spectral resolution of 0.0036 cm^{-1} (250 cm of maximum optical path difference, OPD_{max}) until April 2000 and of 0.005 cm^{-1} ($OPD_{max} = 180$ cm) onward. These MIR spectra are recorded using six optical filters in a sequential manner, a potassium bromide (KBr) beam splitter, and two liquid-nitrogen cooled semiconductor detectors: a photovoltaic indium antimonide (InSb) detector from 1850 to 4500 cm^{-1} and a photoconductive mercury–cadmium–telluride (MCT) detector between 700 and 1300 cm^{-1}. For routine FTIR operations several scans are co-added in order to increase the signal-to-noise ratio; thereby the acquisition of one spectrum takes several minutes.

FTIR solar spectra are only recorded when the line of sight between instrument and the sun is cloud-free. Given the strategic location of IZO, these conditions are very common with an average of 180 d a year of clear days (Cuevas et al., 2019). Thus, FTIR solar measurements at IZO are typically taken two or three times a week (with about two spectra a day for each NDACC optical filter). Although the maximum number of measurement days is concentrated in the warmest months, as shown in Fig. 2, the monthly distribution of sampling days over a year is quite uniform. The total number of NDACC measurement days amounts to 2056 for the 1999–2018 period, with an annual average of $\sim$ 100 measurement days a year.

An overview of the history of the FTIR instruments at IZO is given in Table 1. As previously mentioned, FTIR measurements started in 1999 with the installation of a Bruker IFS 120M. This spectrometer was replaced in 2005 by a more sophisticated model, a Bruker IFS 120/5HR, which continues operating today. During March and April 2005 both instruments measured side by side, which allows the consistency of the spectrometers to be documented (García et al., 2012; Sepúlveda et al., 2012). During the entire operation of the two FTIR systems, they have been placed in air-conditioned scientific containers (Fig. 1c) and been operated in ventilated

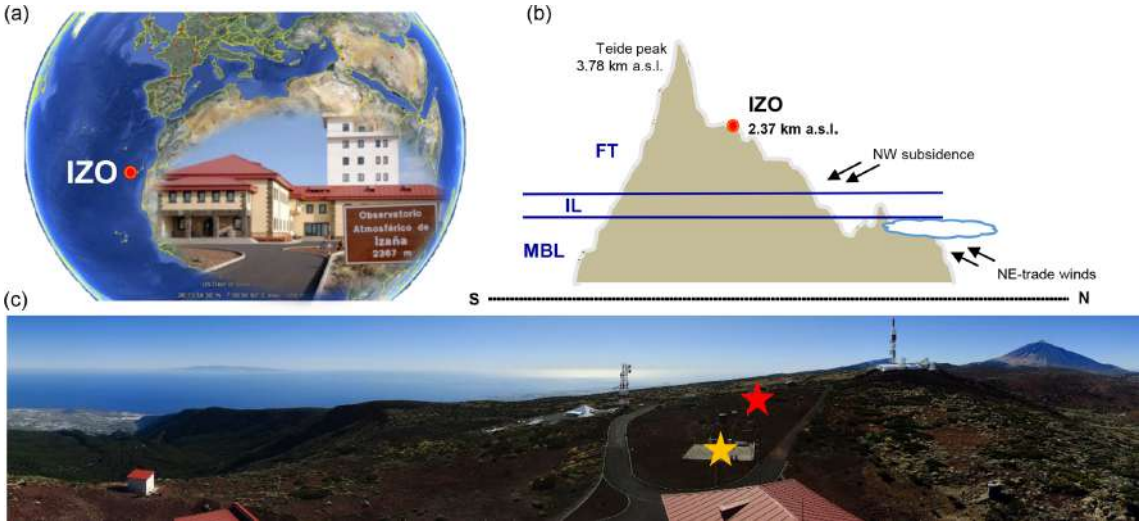

Figure 1. **(a)** Location of IZO in the subtropical North Atlantic Ocean (28.3° N, 16.5° W, on the island of Tenerife). **(b)** Transect of Tenerife island N–S showing the position of IZO and the vertical stratification of Tenerife: MBL – marine boundary layer; IL – inversion layer; and FT – free troposphere. **(c)** Northern and eastern panoramic views of IZO, as observed from the terrace of the observatory's instrumentation tower. Orange and red stars in **(c)** represent the location of the IFS 120M (1999–2005) and IFS 120/5HR spectrometers (2005–present), respectively.

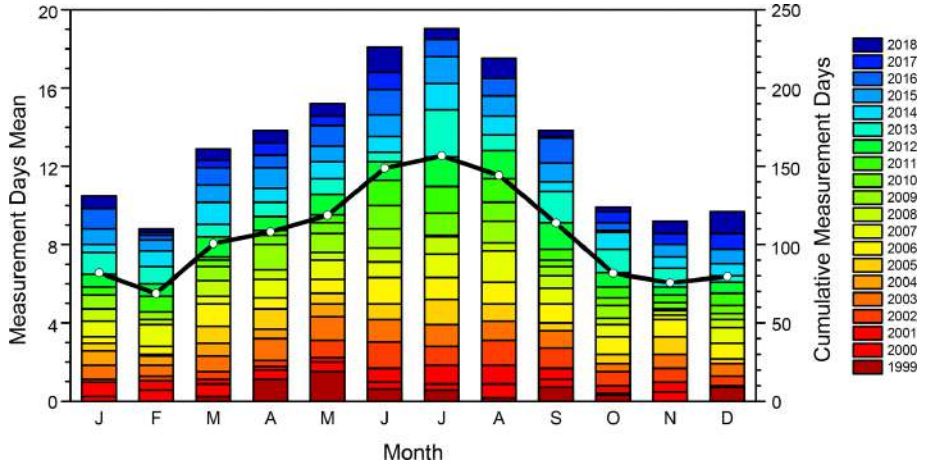

Figure 2. Monthly distribution of NDACC FTIR measurement days from 1999 to 2018. The left axis corresponds to monthly mean of measurement days over the entire period (black line), while the right axis represents cumulative measurement days per month from 1999 to 2018 (coloured scale).

mode (i.e. the spectrometer not evacuated) due to the especially dry conditions at IZO.

The IZO FTIR instruments have been very stable, especially the IFS 120/5HR system, and only two optic realignments have been required during the first 20 years of operation (in June 2008 and February 2013). Apart from that, the most relevant interventions have been the replacement of the internal reference laser used for controlling the sampling of the interferogram in 2016 and 2017, due to frequency instabilities, and the solar tracker upgrade in 2012, when the quadrant-diode set-up was replaced by the CamTracker system (Gisi et al., 2011). By evaluating the image of the sun on the FTIR's entrance field stop acquired by a digital camera, the CamTracker system significantly improves the traditional tracking accuracies (at better than 10 arcsec) and minimizes FTIR pointing errors. In addition, some minor instrumental issues have occurred during these 20 years, causing short data gaps (see Table 1). For further details about the solar FTIR measurements at IZO, refer to Schneider et al. (2005), Sepúlveda et al. (2012), and García et al. (2012).

Table 1. History of the FTIR instruments at IZO with the most important interventions and data gaps.

Date	Intervention
January 1999	Installation of Bruker IFS 120M, start of NDACC observations
June–December 2004	Failure of entrance window
January 2005	Installation of Bruker IFS 120/5HR
March–April 2005	IFS 120M and IFS 120/5HR side-by-side observations
May 2007	Installation of NIR detector (InGaAs), start of TCCON observations
June 2008	Optic re-alignment and recording mode change from AC to DC
November 2009	Installation of laser board ECL03 and optical long-pass filter
December 2009–March 2010	Failure of scanner's motor
November 2010	Installation of laser board ECL04
January 2012	Installation of remote control
April 2012	Update of solar tracker hardware and installation of CamTracker software
February 2013	Optic re-alignment
December 2015	Installation of laser board ECL05
August 2016	Replacement of internal reference He–Ne laser due to frequency instability
October 2016–February 2017	Failure of solar tracker controller
June 2017	Replacement of internal reference He–Ne laser due to frequency instability
September 2017	Replacement of pre-amplification electronics of MIR detectors
December 2018	Replacement of MIR detectors (MCT and InSb)

3.2 Atmospheric remote sensing retrieval principles

By evaluating spectral signatures of vibrational–rotational transitions contained in the solar absorption spectra measured, the FTIR technique allows total column amounts and low-resolution vertical profiles of different atmospheric trace gases to be retrieved with a high degree of precision. For this purpose, refined FTIR retrieval strategies and inversion principles are used, based on the formalism given by Rodgers (2000). In summary, in the inversion procedure, the measurement (solar absorption spectrum) is assembled into a measurement vector $\boldsymbol{y}$, while the unknowns are described by a state vector $\boldsymbol{x}$ and a parameter vector $\boldsymbol{p}$, which define the state of the atmosphere and the auxiliary and instrumental parameters, respectively. These magnitudes are connected by a forward model $\mathbf{F}$ that describes the physics of the measurement process (interaction of solar radiation with the atmosphere):

$$\boldsymbol{y} = \mathbf{F}(\boldsymbol{x}\,,\,\boldsymbol{p}). \tag{1}$$

This is an ill-posed problem; i.e. there are many different atmospheric states ($\boldsymbol{x}$) that produce almost identical spectra ($\boldsymbol{y}$). To overcome this, the solution state is constrained by setting up a cost function:

$$[\boldsymbol{y} - \mathbf{F}(\boldsymbol{x}\,,\,\boldsymbol{p})]^{\mathrm{T}}\mathbf{S}_y^{-1}[\boldsymbol{y} - \mathbf{F}(\boldsymbol{x}\,,\,\boldsymbol{p})] + [\boldsymbol{x} - \boldsymbol{x}_{\mathrm{a}}]^{\mathrm{T}}\mathbf{S}_{\mathrm{a}}^{-1}[\boldsymbol{x} - \boldsymbol{x}_{\mathrm{a}}]. \tag{2}$$

The first term is a measure for the difference between the measured spectrum ($\boldsymbol{y}$) and that simulated for a given atmospheric state ($\boldsymbol{x}$), taking into account the part of the measurement signal which is not explained by the forward model assuming the state $\mathbf{x}$ and parameter values $\boldsymbol{p}$ ($\mathbf{S}_y$ is the covariance matrix of $\boldsymbol{y} - \mathbf{F}(\boldsymbol{x}\,,\,\boldsymbol{p})$). The second term is the regularization term. It constrains the atmospheric solution state ($\boldsymbol{x}$) towards an a priori most likely state ($\boldsymbol{x}_{\mathrm{a}}$), whereby the kind and strength of the constraint are defined by the a priori covariance matrix ($\mathbf{S}_{\mathrm{a}}$). The constrained solution is reached at the minimum of the cost function Eq. (2).

Due to the nonlinear behaviour of $\mathbf{F}(\boldsymbol{x}\,,\,\boldsymbol{p})$, the cost function, Eq. (2), is minimized iteratively by numerical methods. For the $(i+1)$th iteration it is

$$\boldsymbol{x}_{i+1} = \boldsymbol{x}_{\mathrm{a}} + \mathbf{G}_i[\boldsymbol{y} - \mathbf{F}(\boldsymbol{x}_i\,,\,\boldsymbol{p}) + \mathbf{K}_i(\boldsymbol{x}_i - \boldsymbol{x}_{\mathrm{a}})], \tag{3}$$

where $\mathbf{K}$ is the Jacobian matrix (derivatives that capture how the measurement vector $\boldsymbol{y}$ will change for changes in the atmospheric state $\boldsymbol{x}$) and $\mathbf{G}$ is the gain matrix (derivatives that capture how the retrieved state vector $\hat{\boldsymbol{x}}$ will change for changes in the measurement vector $\boldsymbol{y}$).

Because the vertical resolution of a remote sensing FTIR instrument is limited, a proper description of the relation between retrieved and actual state must be provided. This information is theoretically characterized by the averaging kernel matrix ($\mathbf{A}$), which is calculated as $\mathbf{A} = \mathbf{KG}$ and samples the derivatives that capture changes in the retrieved state $\hat{\boldsymbol{x}}$ for changes in the actual atmospheric state $\boldsymbol{x}$. $\mathbf{A}$ links the retrieved and true state as follows:

$$\hat{\boldsymbol{x}} - \boldsymbol{x}_{\mathrm{a}} = \mathbf{A}(\boldsymbol{x} - \boldsymbol{x}_{\mathrm{a}}). \tag{4}$$

Therefore, $\mathbf{A}$ describes the smoothing of the real atmospheric distribution due to the use of a constrained retrieval and thus vertical resolution and sensitivity that can be achieved by a remote sensing FTIR system. While the columns of $\mathbf{A}$ provide the response of the retrieved profile to a perturbation in the state vector, the rows of $\mathbf{A}$ describe the altitude regions that mainly contribute to the retrieved profile

and therefore the vertical distribution of the FTIR sensitivity. As a measure of the total sensitivity, the trace of **A** (also so-called "degrees of freedom for signal", DOFS) gives the number of independent layers discernible by the remote sensing instrument.

Rewriting Eq. (4) and considering potential errors, the retrieved state $\hat{\boldsymbol{x}}$ can be linearized about a reference profile $\boldsymbol{x}_a$ (the a priori profile), the estimated model parameters $\hat{\boldsymbol{p}}$, and the measurement noise ϵ as

$$\hat{\boldsymbol{x}} = \boldsymbol{x}_a + \mathbf{A}(\boldsymbol{x} - \boldsymbol{x}_a) + \mathbf{G}\mathbf{K}_p(\boldsymbol{p} - \hat{\boldsymbol{p}}) + \mathbf{G}\epsilon, \quad (5)$$

where $\mathbf{K}_p$ represents the model parameter Jacobian matrix (i.e. the sensitivity matrix to model parameters). Equation (5) will be the basis for the analytic error estimation of the retrieved NDACC products, where the first term corresponds to the smoothing error associated with the limited vertical sensitivity of the FTIR instrument, the second term accounts for errors due to uncertainties in the input/model parameters, and the third term provides the measurement noise. An extensive treatment of the atmospheric remote sensing retrieval principles is given in Rodgers (2000).

3.3 Retrieval strategies

At IZO the FTIR programme routinely contributes to NDACC with TCs and VMR profiles of ethane (C_2H_6), methane (CH_4), chlorine nitrate ($ClONO_2$), carbon monoxide (CO), hydrogen chloride (HCl), hydrogen cyanide (HCN), hydrogen fluoride (HF), nitric acid (NO_3), nitrous oxide (N_2O), and ozone (O_3) (so-called "standard" products hereafter). All these compounds are retrieved with the non-linear least-squares fitting algorithm PROFFIT (PROFile FIT, Hase et al., 2004), considering the spectral regions and interfering gases given in Table 2. The inversion procedure is solved using a first-order Tikhonov–Phillips regularization (L1, Rodgers, 2000) for all NDACC products, with the exception of $ClONO_2$, which is obtained using a scaling retrieval. The a priori VMR profiles for the target gas and interfering gases are taken from WACCM (Whole Atmosphere Community Climate Model, version 6, http://waccm.acd.ucar.edu, last access: 1 April 2021) provided by NCAR (National Center for Atmospheric Research; James Hannigan, personal communication, 2014). It is important to remark that this a priori information does not vary over time (i.e. on a seasonal or yearly basis), whereby all variability observed in the retrieved NDACC FTIR products comes exclusively from the measured solar spectra. Regarding spectroscopy parameters, these are mainly taken from the HITRAN spectroscopy database (HITRAN2008 with 2009 updates, https://hitran.org, last access: 1 April 2021), with the exception of C_2H_6 and $ClONO_2$, for which specific cross sections or pseudolines are used (Birk and Wagner, 2000; Harrison et al., 2010). Finally, the NCEP (National Centers for Environmental Prediction) 12:00 UT daily temperature and pressure profiles are used for the forward simulations.

All of these settings are based on NDACC-IRWG recommendations (Infrared Working Group, IRWG, 2014) with small modifications. Most relevant changes are those related to CH_4, for which the spectral micro-windows are adopted from Sepúlveda et al. (2014), and the spectroscopy parameters correspond to the improved line list provided by Dubravica et al. (2013). This approach has proved to be less dependent on humidity conditions as it minimizes perturbing H_2O and HDO absorptions and is advantageous for reproducing the tropospheric CH_4 signals (Hase et al., 2011; Sepúlveda et al., 2012, 2014). Another minor modification affects the absorption lines used for O_3 retrievals, which are a simplification of the refined set-up presented by Schneider et al. (2008b). This strategy has been found to provide more precise O_3 estimations than those retrieved from the traditional NDACC approach (1000–1005 cm^{-1} broad micro-window) when comparing to independent measurements (Schneider et al., 2008a, b; García et al., 2021).

In addition to the standard NDACC products, the IZO FTIR programme also contributes to this database with other trace gases (not required by the network, and so-called "non-standard" products hereafter): nitrogen dioxide (NO_2), nitrogen oxide (NO), carbonyl sulfide (OCS), formaldehyde (H_2CO), and water vapour isotopologues ($H_2^{16}O$, $H_2^{18}O$, and $HD^{16}O$). These non-standard NDACC gases are also retrieved with the PROFFIT code, using the settings and references listed in Table 2. Water vapour isotopologue observations have been centrally retrieved and quality-filtered in the framework of the MUSICA project (MUlti-platform remote Sensing of Isotopologues for investigating the Cycle of Atmospheric water; Schneider et al., 2012, 2016; Barthlott et al., 2017). Note that, for the water vapour products, the δ-notation is used to express the relation of the observed isotopologue ratio to the standard ratio VSMOW (Vienna Standard Mean Ocean Water), whereby $\delta D = \frac{HD^{16}O/H_2^{16}O}{VSMOW-1}$ (the ratio for $H_2^{18}O$, δ^{18}, has not been considered in the current work due to very weak signal at IZO; refer to Barthlott et al. (2017) for details about this MUSICA product).

All FTIR products presented here correspond to those publicly available from the NDACC archive (https://www.ndaccdemo.org, last access: 1 April 2021). MUSICA water vapour isotopologues are also available at the NASA LaRC Airborne Science Data for Atmospheric Composition (https://www-air.larc.nasa.gov, last access: 1 April 2021). The only quality filter applied on public FTIR products is that observations taken at high solar zenith angles ($\geq 85°$) have been excluded to avoid imprecise retrievals (mainly caused by misalignments of the solar tracker or spectroscopic issues). These data represent less than 1 % of the total data set.

Table 2. Summary of the spectral regions and interfering gases considered for standard and non-standard NDACC products at IZO. For details about specific retrieval strategies for the non-standard products refer to Vigouroux et al. (2018) for H_2CO, to Schneider et al. (2016) and Barthlott et al. (2017) for water vapour isotopologues, to Hase (2000) and Rinsland et al. (2003) for NO and NO_2, and to Lejeune et al. (2016) for OCS.

Target gas	Micro-windows [cm^{-1}]	Interfering gases	Target gas	Micro-windows [cm^{-1}]	Interfering gases
Standard NDACC products					
C_2H_6	2976.63–2977.06	H_2O, O_3, CH_4	HCN	3268.00–3268.50	H_2O, N_2O, O_3
	2983.10–2985.00			3287.00–3287.40	C_2H_2, CO_2
	2986.46–2986.92			3299.40–3299.60	
CH_4	2611.60–2613.35	H_2O, HDO, CO_2		3315.70–3315.86	
	2613.70–2615.40	NO_2, N_2O, OCS		3331.40–3331.80	
	2835.55–2835.80	HCl, O_3	HF	4000.90–4001.05	H_2O, O_3, CH_4
	2903.82–2903.92			4036.85–4039.08	
	2914.70–2915.15		HNO_3	867.00–870.00	H_2O, CO_2, OCS
	2941.51–2942.22			872.25–875.20	C_2H_2, $CFCl_2$
$ClONO_2$	779.90–780.32	H_2O, C_2H_2, CO_2	N_2O	2481.30–2482.60	H_2O, O_3, CH_4
	779.90–782.38	O_3,HNO_3		2526.40–2528.20	CO_2, N_2O
CO	2057.50–2058.20	H_2O, O_3, CO_2		2537.85–2538.80	
	2069.40–2069.90	N_2O, OCS		2540.10–2540.70	
	2140.40–2141.40		O_3	991.25–993.80	H_2O, CO_2, C_2H_4
	2153.20–2160.00			1001.47–1003.04	$^{668}O_3$, $^{686}O_3$
HCl	2727.73–2727.83	H_2O, O_3, CH_4		1005.00–1006.90	
	2775.60–2775.90	HDO, N_2O, NO_2		1007.348–1009.000	
	2821.40–2821.75	OCS			
	2925.75–2926.10				
Non-standard NDACC products					
H_2CO	2763.42–2764.17	HDO, CO_2, O_3	NO	1900.00–1900.12	H_2O, CO_2, O_3
	2765.65–2766.01	CH_4		1900.49–1900.54	N_2O
	2778.15–2779.10			1903.10–1903.16	
	2780.65–2782.00			2152.00–2152.08	
$H_2^{16}O$	2610.35–2610.80	CH_4, CO_2, O_3,	NO_2	2914.55–2914.74	H_2O, CH_4, O_3,
$H_2^{18}O$	2613.70–2615.40	N_2O, HCl		2925.84–2925.95	HCl
HDO	2626.30–2627.00		OCS	2030.75–2031.06	$H_2^{16}O$,$H_2^{18}O$, CO
	2658.70–2661.80			2047.85–2048.24	$^{12}C^{16}O^{18}O$, CO_2, O_3
	2662.25–2664.35			2049.77–2050.18	
	2712.50–2714.10			2051.18–2051.46	
	2732.050–2732.875			2054.33–2054.67	
	2818.800–2820.125				
	2878.70–2880.70				
	2892.45–2893.45				
	3019.575–3020.200				
	3052.15–3052.75				

3.4 Product characterization: vertical sensitivity and uncertainty budget

The vertical sensitivity of an FTIR system changes significantly from gas to gas, since it depends on the target gas considered, geometry of observation, and instrumental issues (e.g. the signal-to-noise ratio) or retrieval strategy. This fact can clearly be observed in Table 3, which summarizes the DOFS' statistics for all NDACC products. It can be seen that the FTIR vertical sensitivity ranges from roughly resolving four independent layers of O_3 vertical distribution (mean total DOFS of 4.12) to only retrieving information about the TCs of H_2CO, NO_2, and $ClONO_2$ (recall that these gases are retrieved using a scaling retrieval; thereby the total DOFS is theoretically equal to unity). Between two and three atmospheric layers are discernible for CH_4, CO, HCl, HCN, HNO_3, $H_2^{16}O$, N_2O, and OCS, while for C_2H_6, δD, HF, and NO, the sensitivity is limited to one or two layers.

Table 3. Overview of standard and non-standard NDACC products: number of measured spectra (N), mean (M), and standard deviation (σ) of the total DOFS; M and σ of the statistical uncertainty (Sta. unc., in %); and M and σ of the systematic uncertainty (Sys. unc., in %). Note that $H_2^{16}O$ values correspond to the simple MUSICA water vapour product (refer to Sect. 4.3 of Barthlott et al., 2017), while δD products are taken from the quasi-optimal estimation of {H_2O, δD} pair data (refer to Sect. 4.4 of Barthlott et al., 2017). The * refers to those trace gases evaluated using a scaling retrieval.

Gas	N	DOFS M, σ	Sta. unc. [%] M, σ	Sys. unc. [%] M, σ
Standard NDACC products				
C_2H_6	13 625	1.48, 0.15	1.81, 0.39	5.44, 0.17
CH_4	13 625	2.42, 0.14	0.55, 0.09	3.22, 0.06
$ClONO_2$	4323	1.00, 0.00*	105, 1792	94, 1584
CO	5255	3.08, 0.12	0.51, 0.06	2.11, 0.03
HCl	13 625	1.98, 0.19	1.84, 0.44	5.06, 0.16
HCN	3872	2.13, 0.14	11.7, 2.30	16.1, 1.79
HF	4128	1.73, 0.13	1.39, 0.28	5.10, 0.07
HNO_3	5885	2.17, 0.36	2.18, 0.51	8.76, 0.24
N_2O	13 625	2.87, 0.16	0.44, 0.04	2.33, 0.04
O_3	5797	4.12, 0.18	1.79, 0.14	5.05, 0.01
Non-standard NDACC products				
H_2CO	11 124	1.00, 0.00*	52, 19	54, 18
$H_2^{16}O$	12 237	3.13, 0.16	0.94, 0.27	1.21, 0.21
δD	12237	1.71, 0.13	3.21, 1.05	9.78, 2.63
NO	5253	1.48, 0.27	3.75, 1.04	4.55, 0.23
NO_2	13 551	1.00, 0.00*	7.56, 2.07	11.7, 0.64
OCS	5252	2.74, 0.15	1.37, 0.16	2.84, 0.07

These total DOFS values mean that the vertical resolution amounts to roughly 10 km (from the ground up to the middle stratosphere), except for H_2O isotopologues. For the latter, the sensitivity is mainly confined to the troposphere, and the vertical resolution ranges from 2–3 km in the lower troposphere and up to ∼ 8 km in the upper troposphere, as shown in Fig. 3. This figure depicts the rows of the averaging kernel matrix **A** for typical measurement conditions at IZO for all NDACC products, where the A rows of the layers that are well-resolved by the FTIR instrument are identified (and highlighted in coloured lines). For example, for O_3, the four resolvable layers are the troposphere (∼ 5 km), tropopause region (∼ 18 km), the lower stratosphere (∼ 28 km), and the middle stratosphere (∼ 39 km), while for trace gases with total DOFs of about two, such as CH_4 or HCN, the FTIR system basically distinguishes between signals from the troposphere (∼ 5 km) and the stratosphere (∼ 28 km).

The characterization of the retrieved FTIR products is completed by a theoretical assessment of expected uncertainties according to Eq. (5), which evaluates how different sources of errors can be propagated into the retrieved products. At IZO, the error budget, analytically performed by PROFFIT software, includes the impact of measurement noise and the model parameter sources accounting for instrumental/model aspects (baseline parameters, instrumental line shape – ILS – function, solar pointing, atmospheric temperature profiles, solar lines, and spectroscopic parameters), which are split into statistical and systematic contributions. Further details about the uncertainty analysis are given in Appendix A.

Statistics on the uncertainties for all NDACC products are also included in Table 3. The statistical uncertainty mean over the 20-year period (1 standard deviation, σ, in brackets) ranges from ∼ 0.4 % (∼ 0.04 %) for N_2O up to ∼ 50 % (∼ 20 %) and ∼ 100 % (∼ 1800 %) for H_2CO and $ClONO_2$, respectively. The latter, as large values point out, are particularly difficult to retrieve from the solar absorption spectra at IZO due to their weak spectral signature and the relatively low TCs recorded at a subtropical station under background conditions (Kohlhepp et al., 2012; Vigouroux et al., 2018). Overall, statistical uncertainties are dominated by measurement noise, baseline, and atmospheric temperature errors (e.g. Schneider et al., 2008a, 2012; García et al., 2012; Sepúlveda et al., 2012; Vigouroux et al., 2018; García et al., 2021).

A similar pattern is found for systematic uncertainty contributions: H_2CO and $ClONO_2$ present the maximum errors, ∼ 50 % (∼ 20 %) and ∼ 100 % (∼ 1600 %), respectively, while the main water vapour isotopologue $H_2^{16}O$ shows a mean bias lower than 1.5 % (∼ 0.2 %). For all NDACC gases, the systematic uncertainty budget is dominated by spectroscopic errors. In the case of MUSICA water vapour isotopologue products, these are retrieved using an improved spectroscopy based on HITRAN2012, but modifying line intensities (S) and broadening parameters (γ) by about 5 %–10 % (Schneider et al., 2016; Barthlott et al., 2017). This modification is introduced to correct the bias in the water vapour profile products, whereby very small systematic errors are expected.

Figure 4 illustrates how uncertainties in TCs are vertically distributed for all NDACC products. Typically, uncertainty vertical profiles are largely linked to the vertical distribution of each trace gas and FTIR vertical sensitivity (recall Fig. 3). Hence, depending on the target gas, the predominant errors are mainly located in one of the troposphere, upper troposphere–lower stratosphere (UTLS) region, or middle–upper stratosphere layers. Statistical uncertainties between 5 %–10 % are expected in the lower, middle, and upper troposphere for C_2H_6, CO, $H_2^{16}O$, and OCS, and as high as 20 % for HCN tropospheric VMR estimates. HCl, HF, HNO, NO, and OCS are found to be especially sensitive to uncertainties in the UTLS region, while OCS and O_3 exhibit the major error impacts in the middle–upper stratosphere. Large values are also detected in the upper stratosphere for CO and HNO_3, but a subtle impact on the TCs might be expected given the low concentrations of these gases at those altitudes. For CH_4 and N_2O, the error values are mostly limited to ∼ 2.5 % throughout the atmosphere. The systematic

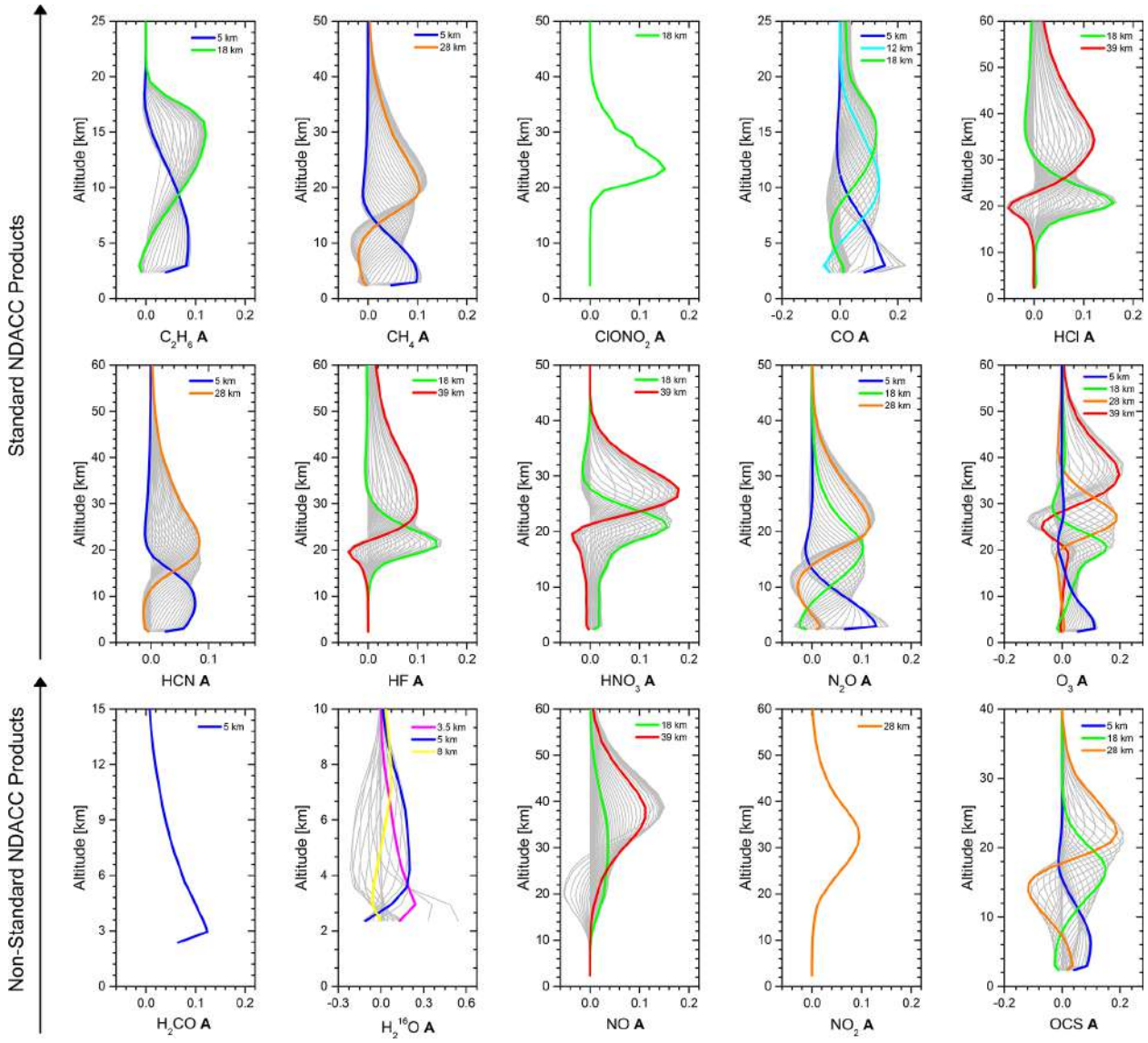

Figure 3. Example of the averaging kernel (**A**) rows, on a logarithmic scale, for standard and non-standard NDACC products for typical measurement conditions at IZO (spectra taken on 20 July 2013 at a solar zenith angle of $\sim 30°$). Note that for H_2O, only the **A** rows of the main water vapour isotopologue ($H_2^{16}O$) are shown. Coloured lines represent **A** rows at altitudes representative of the layers discernible by the FTIR instrument. For a better representation, the ordinate limit for each product has been adapted depending on whether the trace gas has a significant contribution in the middle–upper stratosphere (y limit of 40, 50, or 60 km) or is predominantly distributed in the troposphere–lower stratosphere (y limit of 10, 15, or 25 km).

uncertainties behave similarly to statistical vertical profiles, although in general, the error values are slightly higher. In particular, large error profiles are estimated for H_2CO and $ClONO_2$ and for both statistical and systematic contributions, due to their weak spectral signatures and low abundances at IZO as mentioned above.

4 Long-term performance

The long-term performance of ground-based FTIR instruments can be assessed through indirect tests. Here, the evolution of the instrumental line shape (ILS) function and solar pointing are analysed, as well as the total column-averaged amount of dry air (X_{air}) and of carbon dioxide (XCO_2) retrieved from NDACC FTIR spectra in order to identify instrumental inconsistencies and to document temporal stability of the long-term IZO FTIR time series.

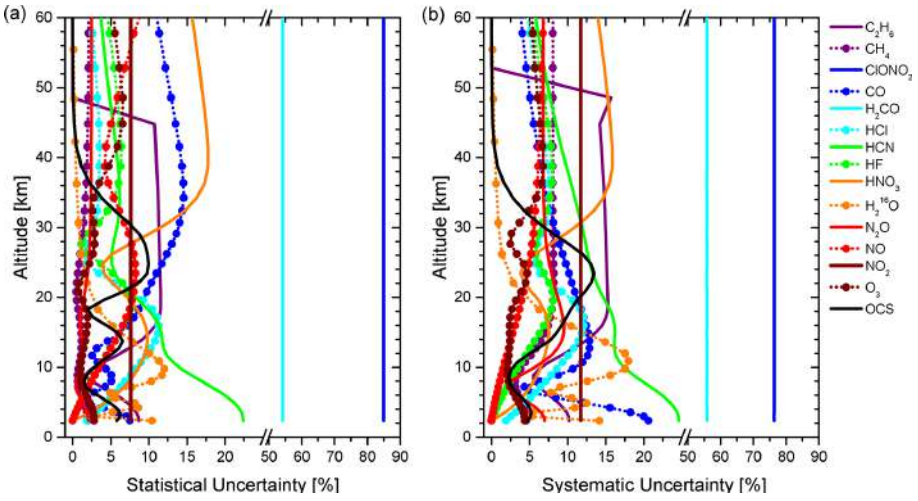

Figure 4. Example of estimated uncertainty profiles for all standard and non-standard NDACC products for typical measurement conditions at IZO (same spectrum as Fig. 3): **(a)** total errors due to statistical uncertainty sources and **(b)** total errors due to systematic uncertainty sources. Total errors are computed as the square root of the quadratic sum of all statistical and systematic error sources considered according to Appendix A. Note that for water vapour only the error profiles of the main isotopologue ($H_2^{16}O$) are shown.

4.1 Instrumental line shape function

A precise knowledge of the ILS function is essential to properly characterize instrument performance, since the ILS affects the absorption line shape on which the retrieved information is based. This is of particular importance when stratospheric gases are concerned due to the fact that the full width at half maximum of their sharp absorption lines and ILS have similar magnitudes (Schneider et al., 2008a, b; García et al., 2021). Therefore, the ILS function at IZO has been routinely monitored about every 2 months since 1999 using re-filled N_2O cells at a pressure of 10 Pa. The ILS is then retrieved from the N_2O absorption lines using LINEFIT software (v14.5), as described in Hase (2012), and applied in the NDACC atmospheric retrievals. Note that the ILS function depends on instrumental configuration (i.e. field stops, detectors, optical filters), thereby at IZO the ILS information is estimated independently for each detector. For the MCT configuration, two broad micro-windows combining saturated and un-saturated N_2O absorbing lines between 1235.0–1279.5 and 1291.8–1301.9 cm^{-1} are used, while for the InSb detector one micro-window between 2173.2 and 2210.0 cm^{-1} is considered (Hase, 2012). In addition, sealed HBr cell measurements have been taken occasionally since 1999.

Continuous monitoring of the ILS function through independent cell measurements ensures that the actual instrumental status is taken into account in NDACC retrievals, but it also allows instrumental alignment and temporal stability to be verified. As an example, Fig. 5 depicts the time series of the ILS's modulation efficiency amplitude (MEA) and phase error (PE) parameters for the NDACC filter 4 measurement settings (InSb detector) for the IZO FTIR instruments between 1999 and 2018. This figure documents that, in addition to suffering from a higher level of spectral noise in the cell and atmospheric measurements, the ILS of the IFS 120M spectrometer is less stable over time than the ILS of the IFS 120/5HR. It further illustrates how punctual interventions on the spectrometers can properly correct the instrumental issues detected: the MEA temporal degradations were mitigated by two punctual optic re-alignments in 2008 and 2013, while the PE asymmetries were minimized by replacing the internal reference laser in 2016 (recall Table 1). In the last years, the IFS 120/5HR has been very stable with a loss of MEA not exceeding 2 % and PE limited to ± 0.04 rad throughout the OPD range. As documented by García et al. (2021), the ILS time series for the MCT configuration is very consistent with that reported for the InSb detector, corroborating proper instrumental characterization of the IZO FTIR instruments.

4.2 Solar pointing

Mispointing of the solar tracker can generate a Doppler shift of solar lines with respect to telluric spectral features due to the solar rotation (Gisi et al., 2011). This effect is considered in the operational NDACC retrievals by fitting a separate shift for solar background lines, whereby effects on trace gas observations are minor. Nevertheless, analysing the Doppler shift also gives a useful method to estimate the solar tracking accuracy. Figure 6a shows the time series of the Doppler spectral scaling factor $\Delta\nu/\nu$, which has been retrieved by observing the solar line shifts in the measured MIR spectra around 2104 cm^{-1} using PROFFIT software. After the quadrant-diode set-up with a semitransparent mirror was installed in February 2005 at the IZO FTIR instrument and fur-

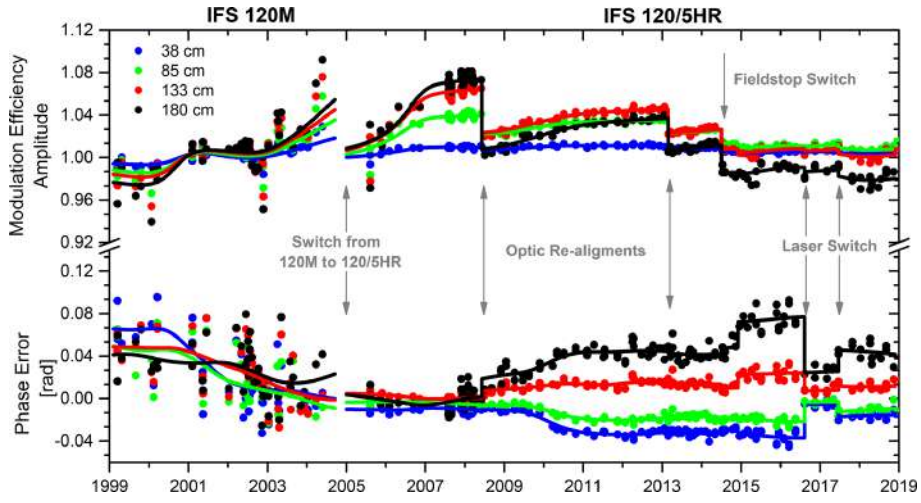

Figure 5. Time series of the modulation efficiency amplitude (MEA) and phase error (PE, in rad) at four OPDs (38, 85, 133, and 180 cm) for NDACC filter 4 measurement settings (InSb detector) of the IZO FTIR spectrometers between 1999 and 2018. Data points represent individual low-pressure N_2O cell measurements, and solid lines show smoothed MEA and PE curves. The solid grey arrows indicate punctual interventions on the instruments: switch from the IFS 120M to the IFS 120/5HR system in 2005, optic re-alignments in June 2008 and February 2013, change of field stop in October 2014, and internal reference laser replacements in August 2016 and June 2017.

ther realignments were made in May 2007, an averaged scaling factor of $\sim 0.18 \times 10^{-7}$ with a scatter of 4.48×10^{-7} was reached. The latter translates into a mispointing precision along the solar equator of ~ 35 arcsec (Gisi et al., 2011). The Doppler scaling values after 2012 clearly indicate the significant improvement induced from the more accurate CamTracker system. The precision is a factor of about 2 lower, and within the range of 20 arcsec. This ensures a minor impact of pointing errors on trace gas retrievals, especially at high observing zenith angles (Gisi et al., 2011).

4.3 XCO_2 and X_{air}

Two approaches based on gas retrievals from the measured MIR spectra have been examined to assess the long-term consistency of NDACC FTIR data sets. The first approach, the XCO_2 method, is based on Schneider et al. (2012), and further elaborated by Barthlott et al. (2015), who demonstrated that the XCO_2 retrievals from NDACC MIR spectra (referred to as NDACC XCO_2 hereafter) can be used as a proxy for the assessment of the network consistency of the NDACC FTIR measurements. This approach compares retrieved NDACC XCO_2 data to a multi-regression XCO_2 model that provides information on long-term, seasonal, and latitudinal behaviour of XCO_2 (Barthlott et al., 2015). To quantify this relationship, the R_{XCO_2} parameter is defined here as follows:

$$R_{XCO_2} = \frac{\text{NDACC } XCO_2}{\text{Modeled } XCO_2}. \quad (6)$$

The XCO_2 model is based on CarbonTracker results and Mauna Loa CO_2 in situ records and adapted to the FTIR measurement site using only latitude and surface pressure as local inputs. On the other hand, the NDACC CO_2 TCs were retrieved by analysing four isolated CO_2 absorption lines between 2620.55 and 2629.95 cm^{-1}, using a scaling retrieval with a fixed WACCM a priori VMR profile and using PROFFIT software. Then, the XCO_2 is calculated by dividing the CO_2 TC by the dry pressure column (DPC) parameter. The DPC is obtained by converting surface pressure (P_S, in pascals) to column air concentration (Sepúlveda et al., 2012; Barthlott et al., 2015), as follows:

$$\text{DPC} = \frac{P_S}{g(\varphi)\mu_{\text{dryair}}} - \text{TC}_{H_2O}\frac{\mu_{H_2O}}{\mu_{\text{dryair}}}, \quad (7)$$

where μ_{dryair} is the molecular mass of dry air ($\sim 28.96 \times 10^{-3}\, N_A$ kg molec.$^{-1}$), μ_{H_2O} the molecular mass of water vapour ($\sim 18.02 \times 10^{-3}\, N_A$ kg molec.$^{-1}$), N_A Avogadro's constant ($\sim 6.022 \times 10^{23}$ molec. mol^{-1}), $g(\varphi)$ the latitude-dependent column-averaged gravitational acceleration, and TC_{H_2O} the water vapour TC. The TC_{H_2O} data are a result of the MUSICA retrieval (Schneider et al., 2012, 2016, and references therein), and surface pressure is taken from NCEP data used in the retrievals. Refer to Barthlott et al. (2015) for further details about the XCO_2 approach.

The second method is based on the X_{air} parameter, which can be used as a sensitive test of the temporal stability of an FTIR instrument because, for X_{air}, there is no compensation of possible instrumental problems (Frey et al., 2019). This quantity compares the measured TC of a well-known, very stable reference gas with surface pressure measurements (Eq. 8). Therefore, for an ideal FTIR instrument X_{air}, values should be close to unity, and large deviations (~ 1 %) from this threshold might indicate instrumental problems (Wunch et al., 2015; Frey et al., 2019). Here, the nitrogen (N_2) ab-

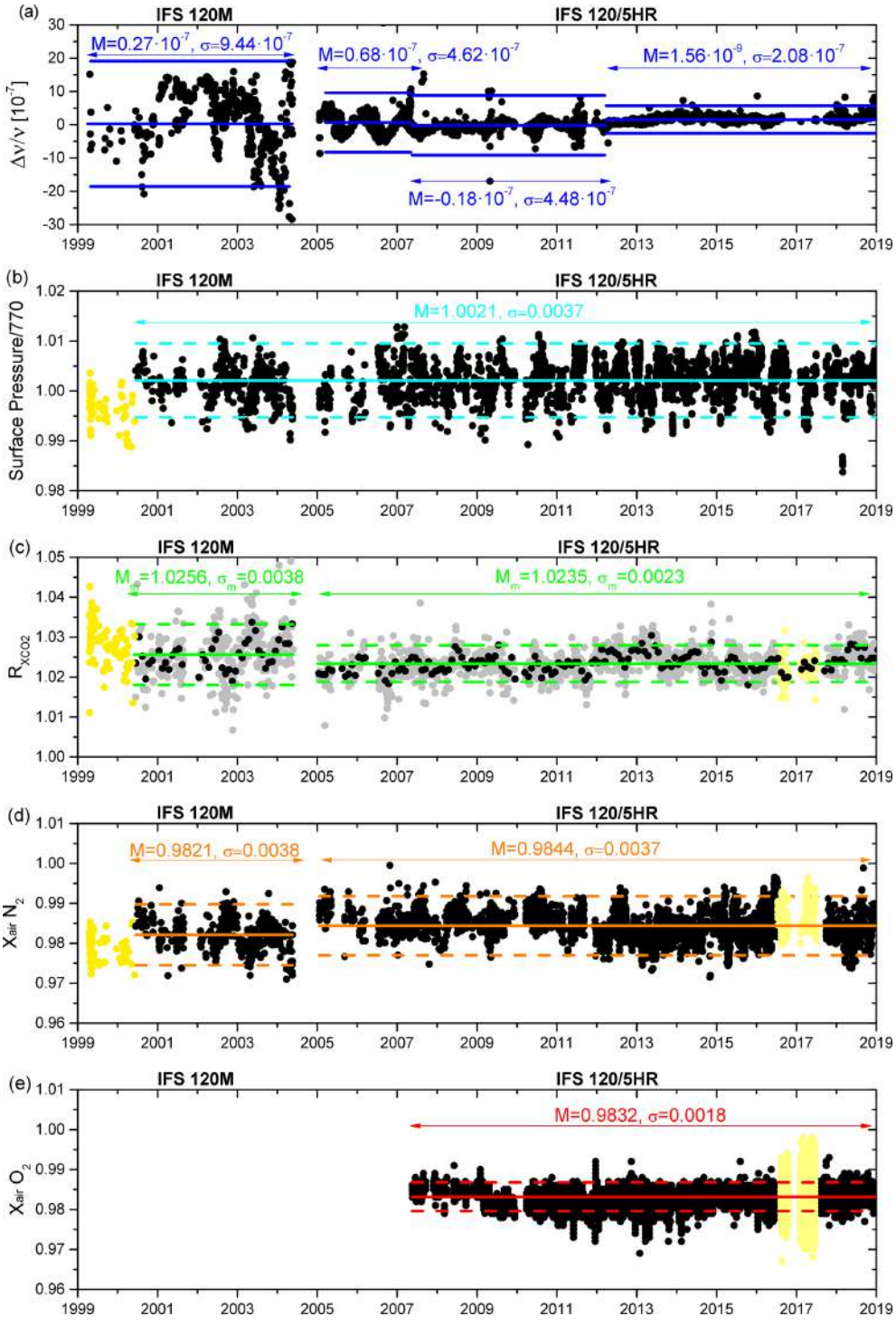

Figure 6. Time series of **(a)** Doppler spectral scaling factor $\Delta\nu/\nu$ estimated from measured MIR spectra around 2104 cm^{-1} solar line; **(b)** surface pressure (normalized by typical surface pressure at IZO of 770 hPa); **(c)** R_{XCO_2} ratio (see definition in the text); **(d, e)** $X_{\mathrm{air}}N_2$ and $X_{\mathrm{air}}O_2$ parameters, calculated using N_2 TCs from the NDACC FTIR spectra and O_2 TCs from the TCCON FTIR spectra, respectively. M_{m} and σ_{m} stand for mean and standard deviation values computed from the monthly time series in **(c)**, while M and σ refer to the same statistics, but based on single measurements in **(d)** and **(e)**. The period marked with yellow dots in **(b)**, **(c)**, and **(d)** denotes instrumental issues on surface pressure records between 1999–2000 and has been ruled out to compute the statistics displayed in the sub-plots. Light-yellow dots in **(d)** correspond to the 2016–2017 period, when frequency instabilities were detected in the FTIR internal reference laser. Solid and dashed lines represent mean values and $\pm 2\sigma$ ranges, respectively.

sorption signatures measured by the NDACC FTIR spectra have been considered as reference gas.

$$X_{\text{air}}N_2 = \frac{F_{N_2}}{TC_{N_2}}\text{DPC}, \quad (8)$$

where F_{N_2} is the dry-air mole fraction of nitrogen in the atmosphere (0.7808) and TC_{N_2} is the N_2 TC. The latter is retrieved by evaluating four N_2 spectral micro-windows between 2403.00 and 2426.3 cm^{-1}, considering a scaling retrieval with a fixed WACCM a priori VMR profile and using PROFFIT software (Goldman et al., 2007).

Figure 6 also shows the time series of the P_S (normalized by the typical surface pressure at IZO of 770 hPa), the R_{XCO_2}, and the $X_{\text{air}}N_2$ parameters. Consistently, both R_{XCO_2} and $X_{\text{air}}N_2$ data are found to be biased by $\sim 2\,\%$ with respect to unity (upward and downward, respectively), which is very likely due to errors in the MIR spectroscopic parameters of the CO_2 and N_2 absorption signatures analysed (Goldman et al., 2007; Barthlott et al., 2015). Therefore, considering $R_{XCO_2} \sim 1.02$ and $X_{\text{air}}N_2 \sim 0.98$ as reference, the XCO_2 and $X_{\text{air}}N_2$ approaches provide consistent results. Anomalous values are detected only in the period 1999–2000, which are attributed to the surface pressure records (marked as grey-white dots in Fig. 6). In 2000, there was a change of type and location of the IZO surface pressure sensor (until June 2000 a Thyas sensor with a precision of ± 1 hPa was used, followed by a Setra sensor with a precision of ± 0.3 hPa), leading to a jump of 0.30 % in both the R_{XCO_2} and $X_{\text{air}}N_2$ parameters. By ruling out this period, the mean $X_{\text{air}}N_2$ values (1σ in brackets) are 0.9821 (0.0038) and 0.9844 (0.0037) for the IFS 120M and IFS 120/5HR, respectively, while for R_{XCO_2} the mean values are 1.0256 (0.0038) and 1.0234 (0.0023) for the IFS 120M and IFS 120/5HR, respectively. These results agree well with the reference $X_{\text{air}}N_2$ and R_{XCO_2} values of 0.98 and 1.02. Note that the reported R_{XCO_2} mean values are computed from the monthly time series as the modelled XCO_2 data cannot capture the synoptic timescale variation (i.e. day-to-day variations) (Barthlott et al., 2015).

The switch of spectrometer from IFS 120M to IFS 120/5HR in 2005 entails the most important change identified in both the $X_{\text{air}}N_2$ and R_{XCO_2} time series, leading to a mean bias of $\sim 0.20\,\%$ between both FTIR instruments. In addition, and consistent with the ILS analysis, the IFS 120/5HR system is found to be more stable than the IFS 120M spectrometer (the R_{XCO_2} scatter is reduced by $\sim 65\,\%$ for the 2005–2018 period and $\sim 3\,\%$ for the $X_{\text{air}}N_2$). However, these differences lie clearly within the estimated confidence ranges for both FTIR systems, and it is, therefore, not expected that they will influence the long-term IZO NDACC time series (e.g. García et al., 2012; Sepúlveda et al., 2012). The other minor instrumental issues or interventions on the FTIR instruments (recall Table 1) do not seem to affect the $X_{\text{air}}N_2$ and R_{XCO_2} time series, since some of them can be partially post-corrected during NDACC gas retrieval processing. That is the case of, for example, the frequency instabilities detected in the internal reference laser in the period 2016–2017. As illustrated in Fig. 6b–c (black–white dots), this issue has an unestimated impact on the R_{XCO_2} and $X_{\text{air}}N_2$ values, because the spectral shift of the measured MIR spectra is simultaneously fitted by PROFFIT software when retrieving the different NDACC products. No significant temporal drifts were detected in either reference time series (at 95 % confidence level), corroborating the long-term temporal stability of the IZO FTIR instruments.

Figure 6 also includes the $X_{\text{air}}O_2$ time series, which is estimated similarly to $X_{\text{air}}N_2$ (Eq. 8) but using the oxygen (O_2) TCs retrieved from TCCON NIR spectra as the reference gas (Wunch et al., 2015). The $X_{\text{air}}O_2$ parameter also suffers from a $\sim 2\,\%$ bias due to O_2 spectroscopic inconsistencies, and a mean typical value of 0.9832 is found for the IZO FTIR instrument. This value is consistent with results reported for other TCCON sites (Wunch et al., 2015). It is worth highlighting that the dispersion for $X_{\text{air}}N_2$ ($\sim 0.37\,\%$) duplicates that found for the IZO FTIR instrument when using the TCCON $X_{\text{air}}O_2$ retrievals (0.18 %). This different behaviour could, in part, be due to the fact that N_2 TCs are retrieved from a few weak N_2 absorption lines $\sim 2400\,\text{cm}^{-1}$, whereby they are more sensitive to spectral measurement noise (and disturbing effects). In addition, discrepancies in the N_2 spectroscopic line lists (e.g. inconsistencies and/or air mass dependencies) could contribute to the reported higher variability. Note also that the $X_{\text{air}}O_2$ and R_{XCO_2} results are very coherent, indicating that the R_{XCO_2} parameter can be successfully used to assess reliability and stability of the NDACC FTIR data.

To sum up, the long-term performance analysis indicates that the IZO FTIR spectrometers do not suffer from major instrumental issues apart from those already identified. In addition, both instruments have been shown to be stable over time (especially the IFS 120/5HR) and well-characterized during their first 20 years of operation. Therefore, the NDACC FTIR trace gas concentrations measured at IZO can be reliably used for long-term climate research.

5 Time series of NDACC total columns

Figure 7 depicts TC time series for all NDACC products recorded at IZO from 1999 to 2018. Together with all the individual FTIR measurements, a time series model fitting the different observations is also displayed. This model combines a linear function with a Fourier time series in order to account for variations on different timescales (linear trend, intra-annual, and inter-annual variations) and is calculated according to Eq. (B1) (see details in Appendix B).

In general, the abundances of trace gases observed at IZO are relatively lower than at middle–high latitudes and in polluted areas due to the special measurement conditions of the observatory. As mentioned above, IZO is a high-altitude station, isolated from local and regional pollution contribu-

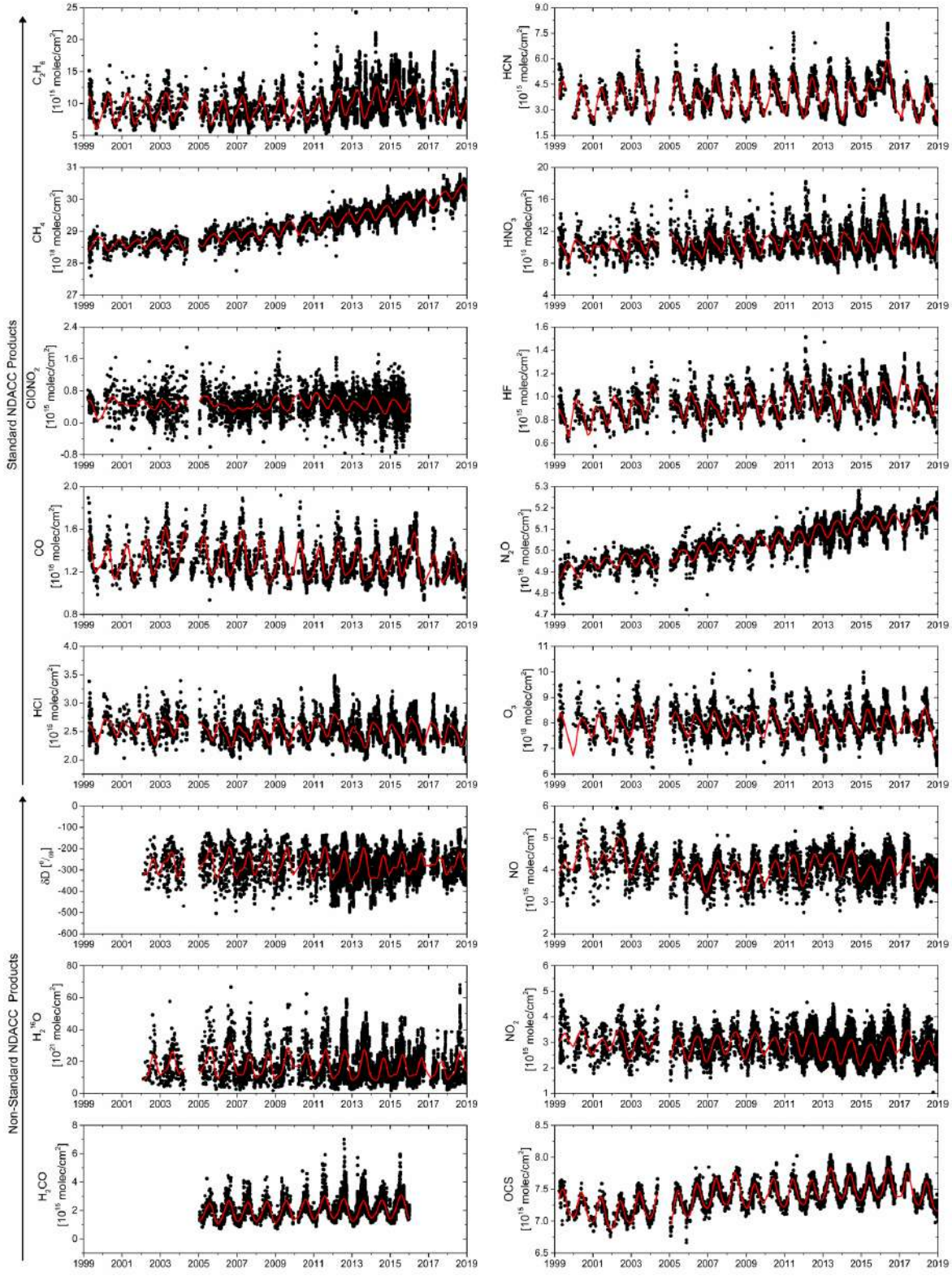

Figure 7. Time series of standard and non-standard NDACC TCs at IZO from 1999 to 2018. Black dots represent all FTIR measurements, while the multi-regression fit of the time series model (see Eq. B1) is depicted as red lines. Data gaps are due to instrumental issues (recall Table 1).

tions, and located in the descending branch of the northern subtropical Hadley cell. Therefore, very low water vapour or pollution-related gas concentrations are typically measured and, for some trace gases, IZO records are close to the FTIR limit of detection (e.g. $ClONO_2$). These typical background conditions are only sporadically disturbed by long-range transport of pollution and/or biomass-burning events from Europe and North America (Cuevas et al., 2013; García et al., 2017, and references therein) and intrusions of polar or tropical streamer air masses causing sporadic downward and upward shift of the UTLS region, respectively (Schneider et al., 2005; Cuevas et al., 2013). These episodes are typically observed in winter when, generally, large variations are also detected in the FTIR TC time series due to a more disturbed atmosphere (see Fig. 7). In addition, direct stratospheric air mass intrusions are occasionally detected in spring and summer (Cuevas et al., 2013), leading to an enhancement of tropospheric concentrations of some trace gases (e.g. O_3). Chemically long-lived gases, such as HF or N_2O, could be used to track these UTLS vertical movements and stratosphere–troposphere exchange (STE) events (Schneider et al., 2005). Figure 7 shows the anti-correlation between the extreme TCs of HF and N_2O, which are more abundant in the stratosphere and troposphere, respectively. This cross-relationship is also noticeable for other stratospheric gases, such as O_3, NO_2, or HNO_3, and tropospheric compounds, like CH_4. On the other hand, during summer, African air masses are frequently advected westwards over the Atlantic Ocean, modifying the atmospheric composition of the lower and middle troposphere of the subtropical North Atlantic region. During these episodes, African boundary layer air is strongly injected into the free troposphere, whereby large mineral dust concentrations are detected at IZO along with industrial pollutants, as well as rather humid, enriched water vapour and relatively low tropospheric O_3 concentrations (Cuevas et al., 2013; González et al., 2016; García et al., 2017, and references therein).

Given the IZO location, the FTIR time series allow changes in the subtropical atmosphere to be investigated, as well as its dynamical and chemical characteristics on different timescales. Apart from the aforementioned short-term episodes, the intra-annual variations are somewhat smooth and are largely dominated by the dynamical shift in the height of the subtropical tropopause, which is associated with stratospheric general circulation. The higher the tropopause, the smaller the relative contribution of the stratosphere to the TCs. This results in minimum (maximum) TCs in summer (winter) for long-lived stratospheric gases (e.g. $ClONO_2$, HCl, HF, HNO_3) and the opposite behaviour for long-lived tropospheric gases (e.g. OCS, N_2O, and CH_4), as seen in Fig. 7. For photochemically active species, such as O_3, NO, and NO_2, seasonal variations are controlled by the joint effect of the height of the tropopause and photochemical reactions, strongly linked to the annual cycle of tropical insolation and middle–stratospheric temperature. These phenomena produce, for example, peak O_3 values in spring and minimum values in autumn–winter at subtropical latitudes. Overall, the range of these averaged seasonal cycles could expand as higher levels are emitted into the atmosphere from biogenic processes, biomass/fossil fuel burning, or other urban/industrial activities.

On a long-term scale, the IZO FTIR time series indicate there is no clear O_3 recovery in the TCs, with no significant linear trend of $-0.04\pm0.17\,\%\,yr^{-1}$ for the period 1999–2018 (here, and hereafter, the trend values are calculated using the monthly time series in order to mitigate sampling effects, according to Eq. (B1), and the error range represents the 95 % confidence level; see details in Appendix B). This steady, long-term behaviour agrees with previous studies as summarized by the latest WMO/UNEP ozone assessment (WMO, 2018, and references therein). This report concluded that no significant trend has been detected in global (60° S–60° N) O_3 TCs over the 1997–2016 period, and statistically significant increases in O_3 had been observed only in the upper stratosphere. The reported stratospheric O_3 recovery of the last decades is directly attributed to the reduction in the production and release of ozone-depleting substances (ODSs), as a response to the Montreal Protocol and its Amendments and Adjustments (Steinbrecht et al., 2017; WMO, 2018, and references therein).

The reduction of ODSs, such as anthropogenic chlorine reservoir species (e.g. HCl and $ClONO_2$), has already been observed in the IZO FTIR time series. As documented in Kohlhepp et al. (2012), a consistent decrease in these compounds by $\sim 1\,\%\,yr^{-1}$ in the period 2000–2009 has been found using globally distributed NDACC FTIR sites, IZO among them. However, recently, an annual increase has been reported of up to 3 % in stratospheric HCl content over the Northern Hemisphere in the period 2007–2012 in contrast with the ongoing monotonic decrease in near-surface emissions (Mahieu et al., 2014). This trend anomaly, also observed in the IZO HCl time series (Fig. 8a), has been attributed to a slowdown in Northern Hemisphere atmospheric circulation. Other stratospheric gases, such as NO and NO_2, seem to also be affected by dynamical changes in the lower/middle stratosphere, showing burden accumulations around the period 2007–2012 (Fig. 8a). This result is consistent with the positive NO_2 trends observed at IZO by Yela et al. (2017), using a refined multi-regression model and a multi-instrument database (ground-based DOAS (differential optical absorption spectroscopy) and FTIR instruments and space-based MIPAS, OMI, and SCIAMACHY sensors). After the 2011 peak, the updated IZO time series suggest a consistent drop for all the stratospheric gases followed by a stabilization of the TCs in the last years. As recently pointed out by Strahan et al. (2020) using NDACC HCl and HNO_3 records at a global scale (including IZO among them), this oscillating behaviour can be caused by an extratropical dynamical variability with a 5–7-year period driven by interactions between transport circulation and the Quasi-Biennial

Oscillation in tropical winds. This work also reveals that the amplitude of this short-term dynamical variability is large in relation to the long-term trend records, whereby it may have a strong impact on trend estimates when using data records that are shorter than multi-decadal. Consistently with other northern NDACC stations (Strahan et al., 2020), the IZO records point to a decline in HCl ($-0.21 \pm 0.19\,\%\,\mathrm{yr}^{-1}$) and an increase in HNO_3 ($+0.44 \pm 0.33\,\%\,\mathrm{yr}^{-1}$) over the 20-year period. However, when considering the 2 decades separately, trends become less apparent and could likely be affected by these short-term dynamical variations as previously mentioned ($+0.41 \pm 0.75\,\%\,\mathrm{yr}^{-1}$ and $+0.19 \pm 0.58\,\%\,\mathrm{yr}^{-1}$ for the periods 1999–2008 and 2009–2018, respectively, for HNO_3 and $-0.17 \pm 0.37\,\%\,\mathrm{yr}^{-1}$ and $-0.14 \pm 0.33\,\%\,\mathrm{yr}^{-1}$ for the periods 1999–2008 and 2009–2018, respectively, for HCl). Note that for a better interpretation of the long-term evolution, Fig. 8 represents the time series of annual TC anomalies relative to the 1999–2018 background signal, which are computed from the measured time series according to temporal decomposition as detailed in Appendix B.

The stabilization of TCs in the last decade is also remarkable for HF. Although fluorine emissions were not explicitly restricted by the Montreal Protocol, and many CFC substitutes contain fluorine, which accounts for the observed increase at the beginning of the 2000s (Fig. 8a), the atmospheric fluorine content has stabilized in response to the progressive implementation of the Montreal Protocol requirements (Kohlhepp et al., 2012; WMO, 2018). As a result, the linear HF TC trend is not significant in the last decade at IZO, $+0.30 \pm 0.41\,\%\,\mathrm{yr}^{-1}$ in the period 2009–2019, compared to a strong positive increment of $+1.84 \pm 0.54\,\%\,\mathrm{yr}^{-1}$ for the period 1999–2008 (the linear trend encompassing the entire period is $+0.98 \pm 0.27\,\%\,\mathrm{yr}^{-1}$).

As controlled ODSs decline, recovery of the stratospheric ozone layer and its long-term evolution largely depends on greenhouse gas concentrations as key modulators of stratospheric temperatures (Steinbrecht et al., 2017; De Mazière et al., 2018; WMO, 2018). The NDACC IZO FTIR time series consistently confirm increasing trends of atmospheric greenhouse gas concentrations widely reported in literature at a global scale (Masson-Delmotte et al., 2021, and references therein) (see Fig. 8b). TC data sets show a linear trend between 1999 and 2018 of $+0.28 \pm 0.01\,\%\,\mathrm{yr}^{-1}$ for CH_4 and of $+0.29 \pm 0.02\,\%\,\mathrm{yr}^{-1}$ for N_2O. The length of the NDACC IZO records also allows a speed-up in the emission rates for CH_4 and N_2O to be observed in the last decade, which is likely caused by the increase in anthropogenic emissions. For CH_4, for example, Bader et al. (2017) found that anthropogenic activities (such as coal mining, gas, and oil transport and exploration) act as secondary contributors to the CH_4 global budget and have played a major role in the increase in atmospheric CH_4 observed since 2005 at a global scale. This acceleration is remarkable for CH_4 with increasing trends of $+0.13 \pm 0.03\,\%\,\mathrm{yr}^{-1}$ and $+0.43 \pm 0.03\,\%\,\mathrm{yr}^{-1}$ for the periods 1999–2008 and 2009–2019, respectively. In the case of N_2O, this phenomenon is also detectable, but to a lesser extent, with linear trends of $+0.26 \pm 0.03\,\%\,\mathrm{yr}^{-1}$ and $+0.31 \pm 0.03\,\%\,\mathrm{yr}^{-1}$ for the periods 1999–2008 and 2009–2019, respectively.

In relation to air quality analysis, the IZO FTIR records of tropospheric pollutants (e.g. CO, C_2H_6, or H_2CO), acquired under background conditions, are well-suited for investigating the effectiveness of the implementation of measures to improve regional and global air quality. In this sense, the long-term behaviour of these gases shows that, while CO records significantly decrease in the period 1999–2018 with a linear rate of $-0.32 \pm 0.21\,\%\,\mathrm{yr}^{-1}$, the H_2CO content increases until 2015 at $+2.2 \pm 0.57\,\%\,\mathrm{yr}^{-1}$, which agrees with the findings of Vigouroux et al. (2018). Then, a smooth drop has been detected from 2016 on, leading to a negative linear trend for the entire period ($-0.71 \pm 0.44\,\%\,\mathrm{yr}^{-1}$ in 2005–2018), consistent with long-term CO behaviour (Fig. 8c). Specific anthropogenic activities can be further monitored through the measurement of related-gas abundances in the atmosphere. This is the case for non-methane hydrocarbons, such as C_2H_6, which shows rather steady values until 2009 when an upturn is detected (Fig. 8c). The causes of this sharp rise, also observed at other globally distributed NDACC FTIR sites, are similar to those documented for the CH_4 increase (i.e. the oil and natural gas production boom in the Northern Hemisphere, particularly in North America) (Franco et al., 2016; Mahieu et al., 2018, and references therein). As with H_2CO, after the 2015 peak the IZO time series suggests a stabilization of the C_2H_6 TCs, at least at subtropical latitudes.

In addition to ozone, greenhouse, and air quality gases, a key element in the Earth's climate is the water cycle. Ground-based FTIR observations of water vapour isotopologue composition have proven to provide valuable information for understanding the different water cycle processes (moisture source, transport, cloud processes, and precipitation) and their relation to climate (e.g. Risi et al., 2012; Schneider et al., 2012; Barthlott et al., 2017; Schneider et al., 2012, 2016, and references therein). Figure 7 also includes column-integrated H_2O and δD time series recorded at IZO, while Fig. 8 displays the corresponding annual anomalies. By analysing the $\{H_2O, \delta D\}$ pair distributions in Fig. 7, distinct lower–middle tropospheric moisture pathways can be identified in agreement with multi-year surface references (Schneider et al., 2016; González et al., 2016): air masses that are clearly affected by dry convection over the African continent (associated with depleted δD and high H_2O values, and more concentrated in summer months); Atlantic dry air masses from high altitudes and high latitudes, as the result of condensation events occurring at low temperatures (characterized by enriched δD and low H_2O concentrations); and Atlantic humid air masses resulting from the mixing with lower-level and more humid air during transport (associated with intermediate δD–H_2O situations).

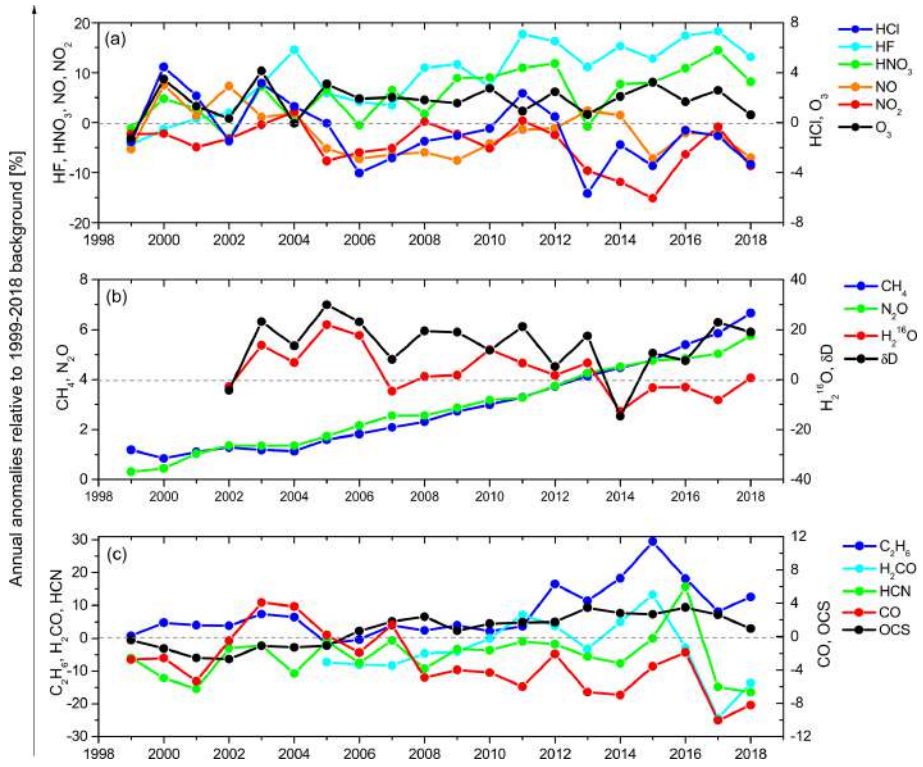

Figure 8. Time series of annual anomalies relative to the 1999–2018 background (in %) for NDACC TCs of **(a)** stratospheric gases (HCl, HF, HNO_3, NO, NO_3, and O_3), **(b)** greenhouse gases (CH_4, H_2O, and N_2O) and δD, and **(c)** tropospheric and air quality gases (C_2H_6, CO, HC_2O, HCN, and OCS). Annual anomalies are computed according to temporal decomposition as detailed in Appendix B.

6 Time series of NDACC VMR vertical profiles

One of the most valuable potentials of NDACC FTIR MIR spectra is the capability of retrieving, albeit roughly, information about the vertical distribution of many trace gases. This is fundamental to monitoring and investigating, for example, the sources and sinks of greenhouse gases and their transport throughout the atmosphere, STE mechanisms, any possible changes of tropospheric and stratospheric chemistry, or the evolution of the ozone layer. Figures 9 and 10 display time series of the IZO FTIR VMR vertical profiles for all NDACC products from 1999 to 2018, where some of the results drawn from the TC analysis are even more clearly observed. This is the case of, for example, the seasonal shift in the subtropical tropopause altitude, resulting in maximum heights in late spring and summer and minimum values in winter. As previously outlined, vertical profiles of chemically stable gases, such as HF or N_2O, can track these seasonal upward and downward movements, and they can identify sporadic episodes on short-term timescales due to the presence of polar or tropical streamer air masses and subsidence stratospheric transport.

Figure 11 illustrates how the vertical information provided by the NDACC FTIR data can be used for long-term analysis at different altitudes, as an example, for O_3, CH_4, and N_2O. In the case of O_3, the steady recovery in TCs found at IZO is likely due to the increase in stratospheric O_3 possibly being partially compensated for by a decrease in O_3 in the troposphere and tropopause regions at subtropical latitudes (e.g. García et al., 2012; Steinbrecht et al., 2017; Gaudel et al., 2018; WMO, 2018, and references therein). In the framework of the SPARC/LOTUS (Stratosphere-troposphere Processes And their Role in Climate/Long-term Ozone Trends and Uncertainties in the Stratosphere, https://www.sparc-climate.org/activities/ozone-trends, last access: 1 April 2021) activity, Steinbrecht et al. (2017) found significant O_3 increases in the upper stratosphere (~ 42 km) by $+0.1\,\%\,yr^{-1}$ to $+0.3\,\%\,yr^{-1}$ outside the polar regions by analysing O_3 profile trends at a global scale over the period 2000 to 2016 from several merged satellite O_3 data sets and from different ground-based NDACC techniques (including the IZO FTIR records). At tropospheric levels this work has also documented that O_3 trends have been smaller and not statistically significant since 2000.

In addition, within the first TOAR (Tropospheric Ozone Assessment Report, https://igacproject.org/activities/TOAR, last access: 1 April 2021) and encompassing all current tropospheric O_3 measurement techniques (surface, sondes, aircraft, lidar, FTIR, Umkehr Dobson and Brewer, satellite, and IZO FTIR records among them), Gaudel et al. (2018)

assessed the present-day distribution and trends of tropospheric O_3 relevant to climate and evidenced that today there is no consistent picture of O_3 tropospheric changes around the world. Although some techniques have pointed to a tropospheric O_3 enhancement since the 1970s in the free troposphere, when focusing on the period from 2000 on, significant uncertainties and discrepancies show up. These findings are consistent with the latest WMO/UNEP report (WMO, 2018), and the results obtained from O_3 profile trends at IZO for the period 1999–2018: a decline in O_3 is detected in the troposphere and tropopause regions ($-0.20 \pm 0.38\,\%\,yr^{-1}$ and $-0.22 \pm 0.43\,\%\,yr^{-1}$ in the 2.37–5.6 and 12–22 km layers, respectively), while an enhancement in O_3 is observed in the stratosphere ($+0.12 \pm 0.15\,\%\,yr^{-1}$ and $+0.03 \pm 0.15\,\%\,yr^{-1}$ in the 22–29 and 29–45 km layers, respectively). However, all these linear trends are not found to be significant at the 95 % confidence level. This may, in part, be induced by the smooth O_3 recovery observed and expected at tropical and subtropical regions (when compared to higher latitudes; Steinbrecht et al., 2017; WMO, 2018), but also by the large year-to-year O_3 fluctuations exhibited in the 2000s (Fig. 11a). As the figure also illustrates, stratospheric O_3 recovery at IZO is clearly visible from 2010 on, consistent with the long-term analysis reported in literature (Steinbrecht et al., 2017; WMO, 2018; De Mazière et al., 2018). The onset of tropospheric O_3 increases also becomes apparent from the end of the 2000s ($+0.68 \pm 0.54\,\%\,yr^{-1}$ in the 2009–2018 period). Finally, it should be pointed out that stratospheric O_3 seems to reflect the observed long-term behaviour of the pivotal species controlling the chemical cycles of O_3 destruction and formation (e.g. chlorine reservoir species, nitrogen oxides; recall Fig. 8a).

For greenhouse gases, the long-term TC tendency is largely the result of the increase in the tropospheric concentrations, where the NDACC products provide similar positive rates in the 1999–2018 period: $+0.30 \pm 0.02\,\%\,yr^{-1}$ and $+0.29 \pm 0.01\,\%\,yr^{-1}$ in the 2.37–5.6 km layer for CH_4 and N_2O, respectively. This monotone increment is also reported in the lower–middle stratosphere (see Fig. 11b), although marked year-to-year fluctuations are detected, likely due to atmospheric transport processes and dynamical mechanisms, as pointed out in Sect. 5. Although greenhouse gas concentrations in the stratosphere are significantly lower than in the troposphere, stratospheric accumulation rates have been found to be significantly greater ($+0.52 \pm 0.08\,\%\,yr^{-1}$ and $+0.50 \pm 0.16\,\%\,yr^{-1}$ in the 22–29 km layer for CH_4 and N_2O, respectively). This result is expected since vertical transport and mixing mechanisms are considerably faster than their respective destruction processes in the stratosphere (i.e. mainly photodissociation for N_2O and oxidation by reaction with hydroxyl radical OH for CH_4). This long-term behaviour, and possible short-term variations, may play an important role in modulating stratospheric temperatures and thus affecting the stratospheric chemical cycles (e.g. enhancing the recovery of stratospheric O_3; Steinbrecht et al., 2017).

For other trace gases, the information drawn from the TC analysis only would cover up the vertical distribution of long-term patterns. This is the case of the tropospheric CO records, whose decrease rate is almost 3 times that for TC abundances: $-0.96 \pm 0.26\,\%\,yr^{-1}$ in the 2.37–5.6 km layer for the 1999–2018 period. This example, together with those described above, further emphasizes the added value of the vertical information provided by the NDACC FTIR data. Nonetheless, it is fair to admit that the trend estimations of short-lived gases, such as CO, might be influenced by the FTIR sampling effects (as addressed in detail in Sect. 8.4).

7 Other climate research applications

Examples of scientific applications of the IZO FTIR time series are described in detail in Sects. 5 and 6, especially those of use in investigating greenhouse gas budgets and long-term changes in key atmospheric gases, such as ozone, chlorine and fluorine compounds, air quality gases, etc., at both the regional and global scales. In addition, the validation of remote observations measured by different satellite instruments has been one of the priorities of the IZO FTIR programme. The high-quality NDACC FTIR data at IZO have been applied extensively for many years in the evaluation of $ClONO_2$, O_3, HNO_3, H_2O, and isotopologues measured by MIPAS (e.g. Höpfner et al., 2007; Blumenstock et al., 2013; Risi et al., 2012); CO, NO_2, H_2O, and isotopologues retrieved by SCIAMACHY (e.g. Risi et al., 2012; Scheepmaker et al., 2015; Robles-González et al., 2016; Yela et al., 2017); CO and HNO_3 observed by ACE-FTIR (e.g. De Mazière et al., 2018, and references therein); O_3 and NO_2 measured by OMI and GOME (e.g. Viatte et al., 2011; Robles-González et al., 2016); CO, H_2CO, and CH_4 measured by TROPOMI (e.g. Borsdorff et al., 2018; Vigouroux et al., 2020; Sha et al., 2021); and O_3, N_2O, CH_4, CO, H_2O, and isotopologues measured by IASI (e.g. Viatte et al., 2011; Schneider et al., 2016; García et al., 2016, 2018). It is worth highlighting that IZO FTIR products, acquired in the framework of TCCON, have also been widely used for satellite validation applications (e.g. Scheepmaker et al., 2015; Borsdorff et al., 2018; Sha et al., 2021, and references therein).

Another important contribution of the FTIR observations is the evaluation and development support of global atmospheric chemistry climate models (CCMs). NDACC IZO data have allowed the performance of many different CCMs to be assessed: KASIMA (e.g. Schneider et al., 2005; Kohlhepp et al., 2012), SLIMCAT (e.g. Schneider et al., 2005; Kohlhepp et al., 2012), EMAC (e.g. Kohlhepp et al., 2012), SOCOL (e.g. Kohlhepp et al., 2012), LMDZ (e.g. Risi et al., 2012), IsoGSM (e.g. Schneider et al., 2012), GEOS-Chem (e.g. Mahieu et al., 2014; Bader et al., 2017; Zhou et al., 2019), and CCMVal initiative (e.g. Steinbrecht et al., 2017). Although the model estimates and measurements are generally consistent, there are still significant discrepancies,

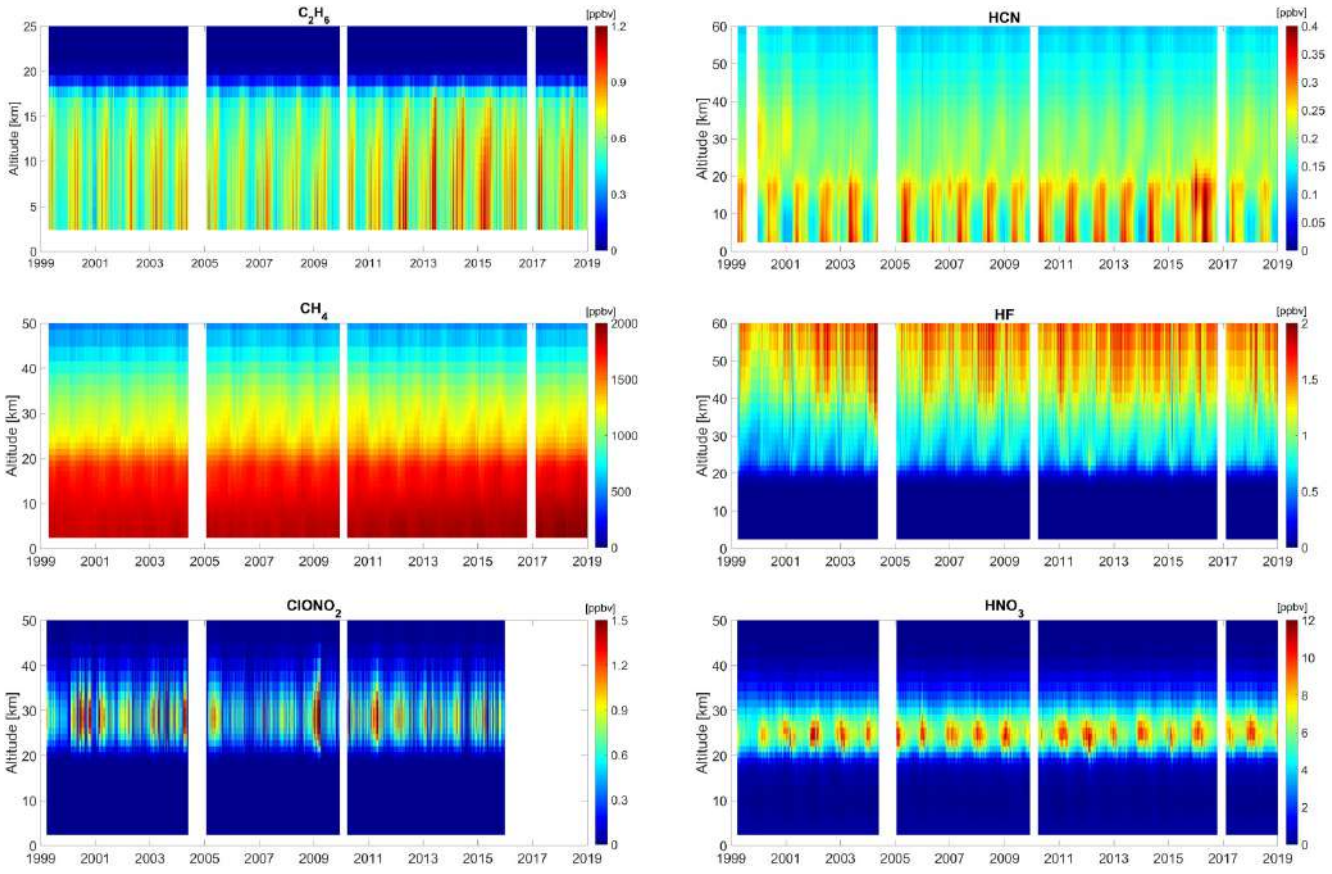

Figure 9. Time series of NDACC VMR vertical profiles at IZO from 1999 to 2018: C_2H_6, CH_4, $ClONO_2$, HCN, HF, and HNO_3. Ordinate limits as in Fig. 3. Also note that the range of the coloured scale, showing VMR concentrations, has also been adapted for each trace gas. White areas correspond to data gaps due to instrumental issues (recall Table 1).

mainly due to the poor representation of the dynamical transport, from local to hemispheric scales, in CCMs. Therefore, the synergy of long-term FTIR observations and simulations may allow for better, deeper understanding of dynamical transport and chemical processes in the atmosphere.

8 Comparison to other reference observations

Quality assessments of different IZO NDACC FTIR products have been partially carried out by previous works (e.g. Schneider et al., 2008a; García et al., 2012; Sepúlveda et al., 2012, 2014; Robles-González et al., 2016; García et al., 2021). Nevertheless, such activities have focused on specific time periods, trace gases, and the application of different approaches. Here, the documentation of the quality and long-term consistency of the IZO NDACC FTIR products is presented by using all reference observations available at IZO within the period 1999–2018 and the same comparison strategy, whereby the results are directly comparable. Note that this comparison exercise is performed only for those NDACC trace gases for which other high-quality measurement techniques are available at IZO, i.e. CH_4, CO, H_2O, NO_2, N_2O, and O_3.

8.1 IZO trace gas observations

The following is a brief description of the reference observations used for comparison to the FTIR records. Refer to Cuevas et al. (2019) for further details about the different measurement techniques and data sets.

1. *Ozone total columns*. O_3 TC observations are routinely performed with Brewer spectrometers from 1991 on, contributing to NDACC since 2001. Since 2003, IZO has acted as the Regional Brewer Calibration Centre for Europe within the WMO, which guarantees the high performance of its O_3 activities. By measuring solar ultraviolet absorption spectra, the IZO RBCC-E reference instruments provide O_3 TCs with an uncertainty of ~ 1 Dobson unit (DU) (Gröbner et al., 2017). Together with Brewer data, O_3 TCs have also been measured at IZO with the DOAS (differential optical absorption spectroscopy) technique since 1993 and within NDACC since 1999 by INTA (Spanish National In-

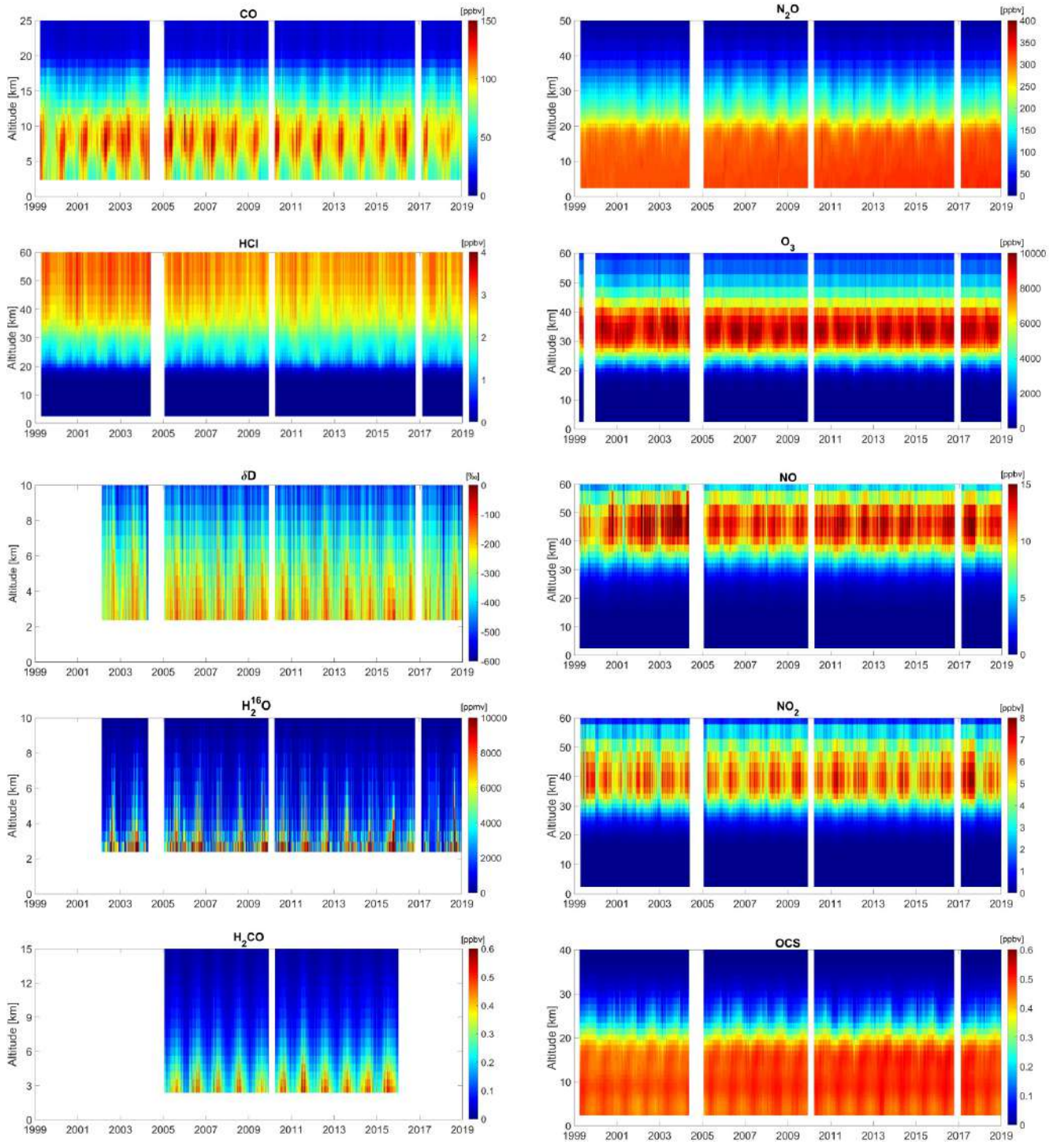

Figure 10. As for Fig. 9, but for CO, HCl, δD, $H_2^{16}O$, H_2CO, N_2O, O_3, NO, NO_2, and OCS.

stitute for Aerospace Technology, https://www.inta.es, last access: 1 April 2021). Based on this technique, a RASAS instrument was installed at IZO from 1998 to 2010, when it was replaced by a MAX-DOAS (multi-axis DOAS) spectrometer which is still in operation (RASAS-II; Robles-González et al., 2016; Yela et al., 2017, and references therein). By analysing scattered light at zenith during twilight (solar zenith angle range of 89–91°), the DOAS approach provides O_3 TCs with an expected precision of ~ 5 %. Nevertheless, compar-

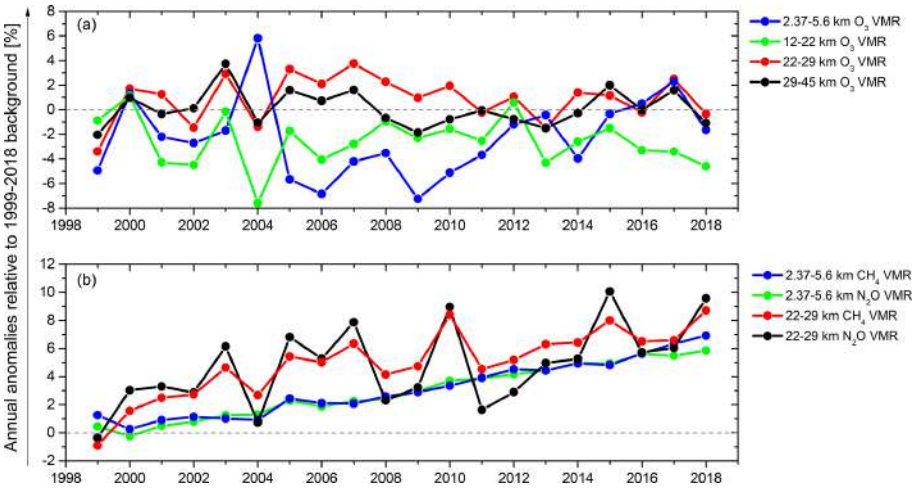

Figure 11. Time series of annual anomalies relative to the 1999-2018 background (in %) for NDACC VMR means of **(a)** O_3 (2.37–5.6, 12–22, 22–29, and 29–45 km layers) and **(b)** CH_4 and N_2O (2.37–5.6 and 22–29 km layers). Annual anomalies are computed according to temporal decomposition as detailed in Appendix B.

isons between Brewer and DOAS O_3 TC records at IZO show an agreement between techniques within 1 % with a standard deviation of only 3 % (Gil-Ojeda et al., 2012).

2. *Nitrogen dioxide total columns*. NO_2 TCs have also been acquired with the DOAS technique since 1993, and in the framework of NDACC since 1998, by INTA. The estimated overall uncertainty in the individual NO_2 TC measurements is expected to be, on average, ~ 12 % (Robles-González et al., 2016; Yela et al., 2017, and references therein).

3. *Methane, carbon monoxide, and nitrous oxide total columns*. CH_4, CO, and N_2O TCs have been routinely retrieved from the FTIR NIR spectra acquired in the framework of TCCON since 2007 (Blumenstock et al., 2017). The TCCON FTIR products are retrieved with the GGG Suite software package (current version GGG2014), whose core part is the non-linear least-squares fitting algorithm GFIT (Wunch et al., 2015). It basically performs scaling retrievals with respect to the a priori VMR profiles to compute TCs of CH_4, CO, and N_2O, together with CO_2, H_2O, HDO, and HF. In order to minimize the impact of instrumental issues on the precision of the TCCON products, retrieved column abundances are converted to total-column-averaged dry-air mole fractions (XGas) by using simultaneously retrieved O_2 TCs. The XGas mole fractions are then calibrated onto the WMO's gas standard scale maintained by NOAA (National Oceanic and Atmospheric Administration, https://www.noaa.gov, last access: 1 April 2021) and provided as standard TCCON products (Wunch et al., 2011, 2015). The calibration factors with respect to the WMO references are estimated by comparing the TCCON retrievals to coincident airborne in situ profiles, leading to values of 0.9765 ± 0.0020 for $X\mathrm{CH_4}$, 1.0672 ± 0.0200 for $X\mathrm{CO}$, and 0.9638 ± 0.0100 for $X\mathrm{N_2O}$ (Wunch et al., 2015). Although TCCON and NDACC FTIR observations are performed with the same instrument at IZO, the measurement settings (spectral range, spectral resolution, detectors, filters, field stop, etc.) and posterior analysis (retrieval software and procedure) are completely different. Thereby, both FTIR data can be considered independent data sets, and thus, TCCON FTIR observations can be a valid reference for the quality assessment of NDACC FTIR data.

4. *Water vapour total columns*. H_2O TC measurements, or equivalent precipitable water vapour (PWV) amounts, are taken at IZO by many different measurement techniques. In fact, in 2014, IZO was appointed by the WMO as a CIMO (Commission for Instruments and Methods of Observation) Testbed for Aerosols and Water Vapour Remote Sensing Instruments, recognizing the high quality and long-term experience of its water vapour measurement programme (Cuevas et al., 2019). The current study only uses those measurements obtained from CIMEL sun photometers within AERONET (since 2003), FTIR within TCCON (since 2007), Vaisala RS92 radiosondes (since 2008), and Global Positioning System (GPS) receivers (precise orbits since 2009). Although meteorological radiosonde measurements have been routinely launched on Tenerife since 1994, here we work with the Vaisala RS92 data that have been processed by the GRUAN (GCOS – Global Climate Observing System Reference Upper-Air Network, https://www.gruan.org, last access: 1 April 2021)

lead centre, which are only available from 2008 on. This limits the comparison data set; however GRUAN data processing ensures that the obtained humidity, pressure, and temperature profiles are well-calibrated and highly accurate (Borger et al., 2018, and references therein). The estimated PWV precision of these techniques is 10 % for CIMEL, 0.7 mm ($\sim$ 10 %–20 % for IZO typical conditions) for GPS, and $\sim$ 6 % for the GRUAN Vaisala RS92 sondes (Schneider et al., 2010; Weaver et al., 2017, and references therein), while for TCCON FTIR H_2O products (XH_2O) a scale factor of 1.0180 ± 0.0040 has been determined using coincident meteorological radiosoundings at globally distributed TCCON sites (Wunch et al., 2015). Recently, at IZO, further studies have corroborated these results, obtaining a mean bias of -0.006 mm (-1.3 %) when comparing TCCON FTIR PWV values to those obtained from meteorological radiosondes launched on Tenerife and processed according to the GRUAN scheme (Almansa et al., 2020). Note that all these PWV techniques are located at IZO, with the exception of meteorological radiosondes, which have been launched twice daily (at 11:15 and 23:15 UT) very close to IZO: from the Santa Cruz de Tenerife station (WMO station 60020, 35 km northeast of IZO) until 2002 and from the Guimar station since then (WMO station 60018, 15 km south of IZO).

5. *Ground-level greenhouse and carbon cycle gases*. Continuous surface measurements of CH_4 (since 1984), and N_2O (since 2007) have been routinely carried out at IZO in the framework of the GAW-WMO programme. CO (since 2008) has also been monitored as it affects the CH_4 cycle. All of these gases are measured by gas chromatography (GC) techniques (CH_4 with a GC DANI 3800, N_2O with a GC Varian 3800, and CO with a GC Trace Analytical RGA-3), with expected uncertainties of ± 2 ppbv for CH_4, ± 0.2 ppbv for N_2O, and ± 2 ppbv for CO (Cuevas et al., 2019, and references therein).

6. *Water vapour profiles*. The H_2O profiles are obtained from the Vaisala RS92 meteorological radiosondes launched on Tenerife and evaluated according to the GRUAN scheme, with uncertainties typically from 5 % near the ground to values of 5 %–20 % at around 10 km altitude (Borger et al., 2018, and references therein).

7. *Ozone profiles*. The O_3 sonde programme on Tenerife started in November 1992, managed by AEMet, and since March 2001 these activities have formed part of NDACC. The electrochemical concentration cell, ECC, sondes (Scientific Pumps 5A and 6A) were launched once per week from Santa Cruz de Tenerife until 2010 and since then from Puerto de la Cruz (12 km north of IZO). The expected uncertainty of the ECC sondes is ± 5 %–15 % in the troposphere and ± 5 % in the stratosphere (WMO, 2014).

8.2 Comparison strategy

The comparison methodology used here is based on previous works carried out at IZO (e.g. Sepúlveda et al., 2012; García et al., 2012; Sepúlveda et al., 2014; García et al., 2016, 2018) and can be briefly summarized as follows.

1. *Considerations for comparison of remote sensing techniques*. When comparing different remote sensing retrievals, there are multiple factors affecting the comparison, namely, spectral ranges, spectral resolution, retrieval strategies, vertical sensitivity, etc. This is especially critical for the DOAS and FTIR methods since, together with the aforementioned factors, they are quite different measurement techniques sampling different air masses and with different observing geometries (Gil-Ojeda et al., 2012; Robles-González et al., 2016; Yela et al., 2017). On one hand, the DOAS and NDACC FTIR retrievals use a profile retrieval; however while DOAS considers varying a priori VMR profiles for each target gas, they are kept fixed for the NDACC FTIR retrievals. TCCON FTIR concentrations are obtained using a scaling retrieval assuming a priori VMR profiles varying from day to day. On the other hand, the Brewer, CIMEL, and GPS techniques use completely different measurement approaches, which are not based on inverse methods. Other discrepancies or biases arise from the different spectral regions and spectral resolutions used in the different remote sensing techniques. The different measurement approaches and instrument capabilities also lead to different vertical sensitivity. Even using the same instrument and technique, NDACC and TCCON averaging kernels tend to peak at different altitudes, and thus NDACC and TCCON FTIR products may reflect concentration variations from different atmospheric layers. All these aspects can introduce significant differences in the retrieved products and must be considered when interpreting the comparison results (e.g. Barthlott et al., 2015; Robles-González et al., 2016; Kiel et al., 2016, and references therein).

2. *FTIR products*. The FTIR TCs of NO_2 and O_3 are directly compared to the reference IZO data. For H_2O, since the reference techniques considered here do not distinguish between H_2O isotopologues, the MUSICA optimal estimation of $H_2^{16}O$ data (so-called "Type 1" products; Barthlott et al., 2017) were used. The TCCON H_2O TCs were used instead of the standard XH_2O products, and both TCCON and NDACC H_2O TCs were transformed into PWV values to be consistent with the other H_2O techniques. Note that the TCCON PWV values are not post-calibrated with the aforementioned

scale factor, since the latter has been determined for $X\mathrm{H_2O}$, not for $\mathrm{H_2O}$ TCs.

For $\mathrm{CH_4}$, CO, and $\mathrm{N_2O}$, the NDACC TC data were converted to total column-averaged dry-air mole fractions by using the DPC parameter (Eq. 7) in order to be compared to the standardized, WMO-calibrated TCCON XGas retrievals. This transformation also allows the analysis of the capability of the NDACC XGas products to capture tropospheric concentration variations by comparing them to IZO ground-level concentrations. In addition, the IZO ground-level records are compared to the NDACC tropospheric $\mathrm{CH_4}$, CO, and $\mathrm{N_2O}$ concentrations ($\mathrm{CH_{4,TRO}}$, $\mathrm{CO_{TRO}}$, and $\mathrm{N_2O_{TRO}}$, respectively), which are obtained as the mean of retrieved NDACC VMR profiles between IZO altitude (2.37 km a.s.l.) and middle troposphere (5.6 km a.s.l.) (Sepúlveda et al., 2012; García et al., 2014).

In order to compare the FTIR vertical profiles to the in situ highly resolved profiles (meteorological and ECC sondes), the latter have been vertically degraded by applying the averaging kernels obtained in the FTIR retrieval procedure, following Eq. (4). By doing so, the limited sensitivity of the FTIR data is properly taken into account in the comparison (Rodgers, 2000). To homogenize the reference data sets, only those sondes with continuous measurements up to 12 km for $\mathrm{H_2O}$ and up to 29 km for $\mathrm{O_3}$ have been considered. Beyond these altitudes, the sonde profiles have been completed using the corresponding FTIR a priori VMR profiles to compute the smoothed humidity and $\mathrm{O_3}$ profiles.

3. *Temporal criteria*. Temporal collocation depends on the natural variability of each target gas, FTIR uncertainty, and characteristics of each reference technique; therefore it varies from gas to gas.

   For $\mathrm{CH_4}$, CO, and $\mathrm{N_2O}$, the daily night-time means (20:00–08:00 UT) of the IZO ground-level records and the daily day-time means of the FTIR products are paired (Sepúlveda et al., 2012; García et al., 2018). As previously mentioned, the IZO night-time surface data represent the background regional signal of the free troposphere well, while during day-time local air circulations may disturb the ground-level data. In addition, these trace gases show rather small intra-day variations, so a pairing of daily means could be more meaningful than a comparison of individual measurements. A similar temporal criterion is then applied for the $\mathrm{CH_4}$, CO, and $\mathrm{N_2O}$ column retrievals from the NDACC and TCCON data sets; i.e. the daily means of $X\mathrm{CH_4}$, XCO, and $X\mathrm{N_2O}$ are matched.

   Given the large natural variability of $\mathrm{H_2O}$, and in order to ensure that the different techniques observe similar air masses, the temporal coincidence criterion has been restricted to 1 h for all the PWV products (Schneider et al., 2010). For the radiosonde data, the time at half of the observation is chosen as reference time (a sonde takes approximately 1 h between the launch and burst in the UTLS).

   For the Brewer $\mathrm{O_3}$ TC the 1 h temporal coincidence is also applied, since the precision of both the FTIR and Brewer techniques is able to properly resolve the intra-day $\mathrm{O_3}$ concentration variations (Schneider et al., 2008b; García et al., 2016). For the DOAS-FTIR intercomparison, because the DOAS technique measures only during twilight and $\mathrm{O_3}$ and $\mathrm{NO_2}$ are photochemically active species, the FTIR observations are averaged before and after 12:00 UT (morning and afternoon, respectively) (Robles-González et al., 2016).

   Finally, for $\mathrm{O_3}$ profile comparison the strategy described by Schneider et al. (2008a) and García et al. (2012) was followed, where the ECC sondes are corrected daily by means of coincident Brewer data. These works illustrated that by applying this correction, the quality and long-term stability of the ECC sonde data can be significantly improved. Given that intra-day $\mathrm{O_3}$ variability is much lower than that for $\mathrm{H_2O}$, the temporal coincidence window is extended to 3 h around the $\mathrm{O_3}$ sonde launch.

   To avoid redundant data, for all the intercomparisons, each FTIR measurement is only paired once to the reference observation that minimizes the time difference within the temporal coincidence window.

4. *Temporal decomposition*. Once the FTIR and reference IZO observations have been temporally paired, quality assessment of the FTIR products is addressed, both directly comparing the measured data sets and at different timescales by means of a temporal decomposition of the measured time series. This temporal decomposition, explained in detail in Appendix B, provides an added value for comparison as it allows the temporal signals discernible by the FTIR system to be properly identified (i.e. single measurements, daily and seasonal averages, and long-term variations) (Sepúlveda et al., 2012, 2014; García et al., 2016, 2018).

8.3 Direct and timescale comparison

Table 4 summarizes the direct comparison between the NDACC FTIR products and the reference data sets considered: TCs of $\mathrm{O_3}$, $\mathrm{NO_2}$, and $\mathrm{H_2O}$ (PWV); column-averaged amounts of $\mathrm{CH_4}$, CO, and $\mathrm{N_2O}$; and tropospheric $\mathrm{CH_4}$, CO, and $\mathrm{N_2O}$ records. In addition, Figs. 12 and 13 display the time series of paired FTIR and reference observations and the corresponding relative differences (FTIR-Reference), as well as the multi-year seasonal cycles, while Fig. 14 synthesizes the comparisons on different timescales.

1. *Ozone.* Similarly to previous works, an excellent agreement is found between FTIR and Brewer $\mathrm{O_3}$ TCs at

Table 4. Summary of intercomparison between the FTIR products and the IZO reference data sets: reference technique, mean bias (MB, in % and absolute units), standard deviation of the differences (σ, in % and absolute units), slope and intersect of the least-squares fit (Y is FTIR and X is reference), Pearson correlation coefficient (R), number of coincidences (N), and coincident period. The differences are computed with respect to the reference IZO observations: (FTIR − Reference) in absolute units and (FTIR − reference)/reference in %. The * means 10^{14} molec. cm^{-2}. Note "am" refers to morning and "pm" refers to afternoon.

Product	Reference	MB [%]	MB [unit]	σ [%]	σ [unit]	Slope	Intersect [unit]	R	N	Period
O_3 TC	Brewer	3.57	10.5 DU	0.95	2.90 DU	1.04 ± 0.01	-1.54 ± 1.29 DU	0.99	5104	1999–2018
O_3 TC	DOAS am	7.78	22.3 DU	3.07	8.71 DU	0.88 ± 0.03	55.6 ± 8.0 DU	0.89	949	2000–2018
O_3 TC	DOAS pm	9.88	27.9 DU	3.38	9.44 DU	0.87 ± 0.03	62.7 ± 7.3 DU	0.88	1215	2000–2018
NO_2 TC	DOAS am	−0.10	−0.11*	10.8	2.91*	0.67 ± 0.03	8.90 ± 0.95*	0.75	1100	1999–2018
NO_2 TC	DOAS pm	−21.7	−7.77*	10.0	3.82*	0.56 ± 0.03	9.44 ± 1.04*	0.77	1243	1999–2018
PWV	CIMEL	37.9	1.66 mm	11.6	0.95 mm	1.34 ± 0.01	0.37 ± 0.02 mm	0.98	11469	2003–2018
PWV	GPS	27.1	1.02 mm	23.2	0.60 mm	1.08 ± 0.01	0.65 ± 0.02 mm	0.98	11186	2009–2018
PWV	Sonde	17.2	0.72 mm	18.2	0.79 mm	1.02 ± 0.04	0.62 ± 0.22 mm	0.97	154	2008–2017
PWV	TCCON	9.56	0.51 mm	7.63	0.48 mm	1.09 ± 0.01	0.05 ± 0.05 mm	0.99	1127	2007–2018
XCH_4	TCCON	0.23	4.14 ppbv	0.37	6.58 ppbv	0.98 ± 0.02	38.7 ± 38.7 ppbv	0.96	635	2007–2018
XN_2O	TCCON	−0.53	−1.66 ppbv	0.66	2.05 ppbv	0.71 ± 0.03	88.8 ± 9.9 ppbv	0.87	633	2007–2018
XCO	TCCON	6.08	4.61 ppbv	2.70	2.20 ppbv	1.09 ± 0.02	-2.18 ± 1.55 ppbv	0.97	629	2007–2018
$CH_{4,TRO}$	GAW	2.56	47.8 ppbv	1.02	19.2 ppbv	1.03 ± 0.03	-1.91 ± 52.03 ppbv	0.87	1634	1999–2018
N_2O_{TRO}	GAW	0.10	0.35 ppbv	0.54	1.77 ppbv	1.15 ± 0.04	-49.2 ± 12.1 ppbv	0.89	1013	2007–2018
CO_{TRO}	GAW	−13.4	−11.8 ppbv	8.31	7.65 ppbv	0.80 ± 0.03	7.40 ± 2.65 ppbv	0.87	984	2008–2018

IZO. More than 98 % of the O_3 TC variance obtained for both techniques agrees (Pearson correlation coefficient, R, of 0.99, i.e. $R^2 = 0.98$), and the dispersion between techniques is smaller than 1 % (1σ, σ stands for the standard deviation of the relative differences with respect to reference data, i.e. Brewer data). This scatter accounts for the precision of both techniques; thereby it could be considered a very conservative value of FTIR precision.

A large contribution to this dispersion can be attributed to the impact of atmospheric temperature profile uncertainties on the FTIR O_3 retrievals (Schneider et al., 2008a, b; García et al., 2012, 2021). When considering more refined O_3 products (not the standard NDACC product), including a simultaneous temperature profile fit in the O_3 retrieval procedure, the scatter between Brewer and FTIR can be significantly reduced by up to 0.5 %–0.7 % (Schneider et al., 2008b; García et al., 2012, 2021). Although the agreement is very satisfactory, the Brewer and FTIR products differ in their absolute quantification of O_3 TCs: the FTIR is upward biased by ~ 3.6 %. This well-known systematic discrepancy is likely introduced by inconsistencies between ultraviolet and infrared spectroscopic parameters. As presented in Sect. 3.4, uncertainties of 5 % in the HITRAN O_3 spectroscopy may explain a bias of ~ 5 % between FTIR and Brewer data.

Although a direct comparison between coincident DOAS and FTIR instruments is challenging, a satisfactory consistency has been documented for O_3 TCs: the FTIR–DOAS mean difference is ~ 8 %–10 % with a σ of ~ 3 %. These values agree with the expected precision for DOAS (~ 5 %) and with previous DOAS–Brewer comparisons carried out at IZO (Gil-Ojeda et al., 2012). Analogously to Brewer, the bias between techniques is likely due to spectroscopic inconsistencies between the spectral regions.

When examining the different timescale signals, the O_3 TC variations are similarly captured by all techniques at the short-term (measurement-to-measurement) and seasonal scales, as shown in Fig. 12 (right panels) and summarized in Fig. 14. For long-term signals, while Brewer and FTIR observations similarly reproduce the O_3 evolution with a correlation of ~ 95 %, DOAS O_3 observations show a poorer agreement with the FTIR data ($R \sim 60$ %). This is likely due to a systematic bias introduced by the switch of DOAS instrument in 2010 (the change point is clearly recognizable in the difference time series displayed in Fig. 12a). As a result, the DOAS long-term trends (Fig. 14e) are found to overestimate the Brewer and FTIR values. Note that the linear trends shown in Fig. 14e have been computed considering the coincident observations and so could differ from the values presented in Sect. 5, which are based on the FTIR monthly means.

2. *Nitrogen dioxide.* Moderate performance is found when comparing the DOAS and FTIR NO_2 products. The scatter obtained for the relative differences, ~ 10 %, was found to agree well with the expected precision of DOAS NO_2 data (~ 12 %), with the FTIR theoreti-

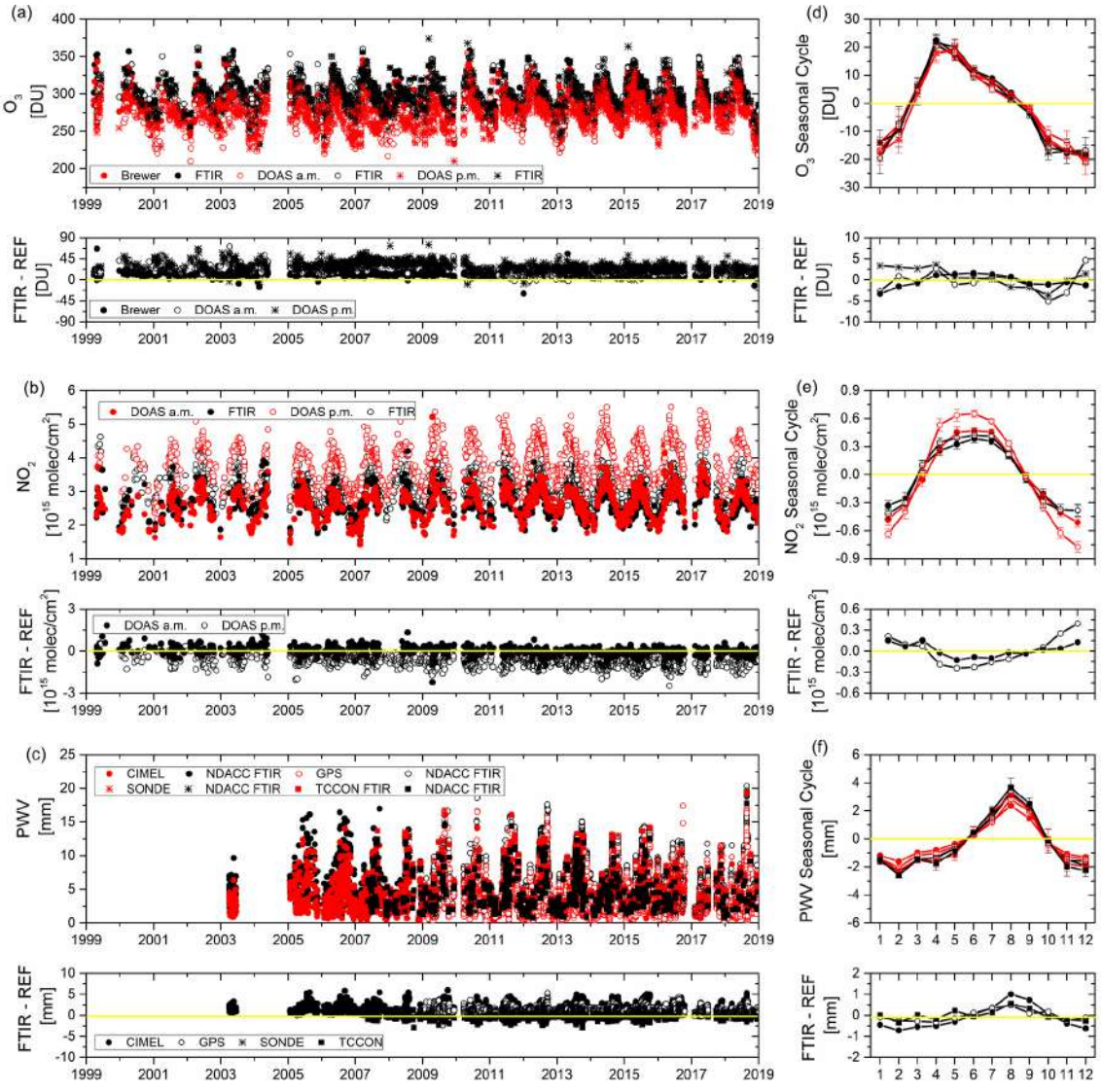

Figure 12. Time series of coincident NDACC FTIR TCs and IZO reference data sets and of differences (FTIR − reference, in absolute units) in the left panels for **(a)** O_3, **(b)** NO_2, and **(c)** PWV. Right panels show the averaged annual cycle of variations relative to the long-term background, from temporal decomposition analysis, and of differences for **(d)** O_3, **(e)** NO_2, and **(f)** PWV. Error bars in annual cycles are standard errors of the monthly mean: $2 \times \sigma/\sqrt{n}$, with σ the standard deviation and n the number of monthly measurements. The yellow line indicates the zero value (i.e. no difference or no annual cycle signal).

cal uncertainty budget (recall Table 3), and with previous works (∼ 9 %–11 %; Robles-González et al., 2016). However, a remarkable asymmetry in the mean differences has been documented between morning and afternoon FTIR–DOAS comparisons for all timescales analysed (Figs. 12 and 14). In general, for both O_3 and NO_2, the DOAS morning observations compare better with the FTIR data than afternoon values. This pattern is largely introduced by diurnal variations in the TCs due to photochemical processes, especially important for active species like NO_2, which are captured differently by the two techniques. A photochemical correction (solar zenith angle-dependent) can be applied to the FTIR data to refer the measurements to the DOAS acquisition time, which reduces the bias between the techniques and the morning–afternoon asymmetry (Robles-González et al., 2016). In addition, part of these differences can be attributed to the different vertical sensitivities of the DOAS and FTIR techniques: while the DOAS method, with zenith-sky measurements at twilight, is almost insensitive to troposphere and tropopause regions (Gil-Ojeda et al., 2012; Robles-González et al., 2016), the FTIR system can detect UTLS contributions (recall Fig. 4).

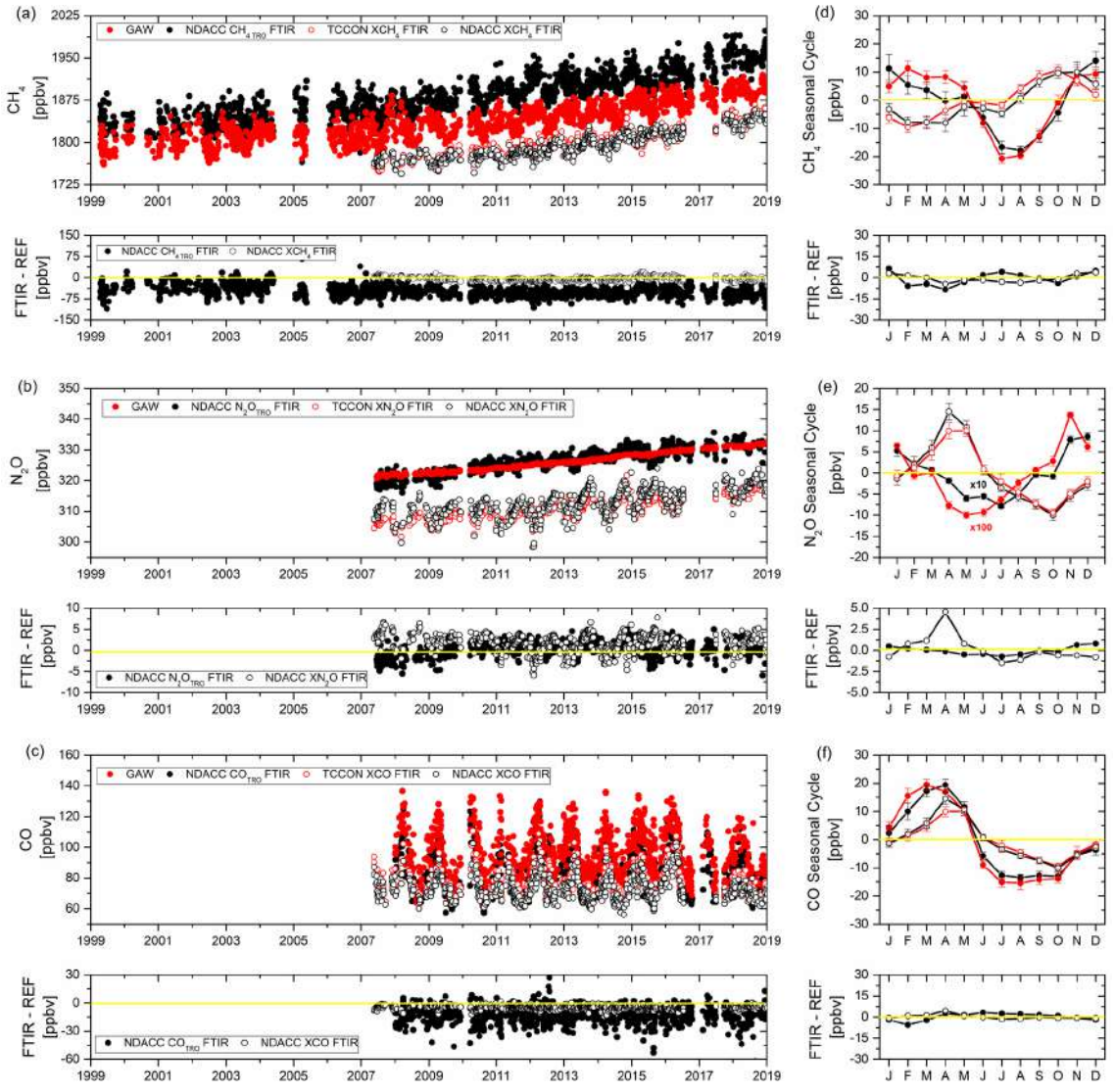

Figure 13. As for Fig. 12, but for tropospheric and column-averaged NDACC products: **(a, d)** CH_4, **(b, e)** N_2O, and **(c, f)** CO.

The diurnal asymmetry might be the reason for the inconsistency between the FTIR morning and afternoon records for the long-term signals. While the FTIR morning observations point to a significant NO_2 increase over IZO (similar to that for DOAS data), the FTIR afternoon records seem to indicate the opposite long-term behaviour (Fig. 14e). However, further studies would be recommended to better understand what drives the difference in these linear trends and reconcile them.

3. *Water vapour.* The consistency between the NDACC PWV product and the other PWV techniques is very satisfactory, with variances of more than 95 % in agreement. As expected, the best performance is found for FTIR PWV products acquired within TCCON (correlation higher than 0.99 and scatter of ~ 8 %), consistent with previous comparisons at globally distributed FTIR sites (e.g. Weaver et al., 2014). The degree of comparability with the other sun-photometer technique considered (AERONET CIMEL) is also high, with a dispersion of ~ 12 %, while larger scatter values are obtained for the other rather different PWV techniques (18 % and 23 % for sondes and GPS, respectively). These values are very close to the estimated precision of each measurement technique (recall Sect. 8.1) and are found to be very consistent with previous PWV comparison works carried out at IZO (Schneider et al., 2010; Almansa et al., 2020). These studies comprehensively compared FTIR PWV retrievals with different techniques (MFRSR, CIMEL, EKO, GPS, and sondes), highlighting the different observing geometries (i.e. sampling different air masses) and atmospheric conditions (humid or dry), and the significant clear-sky

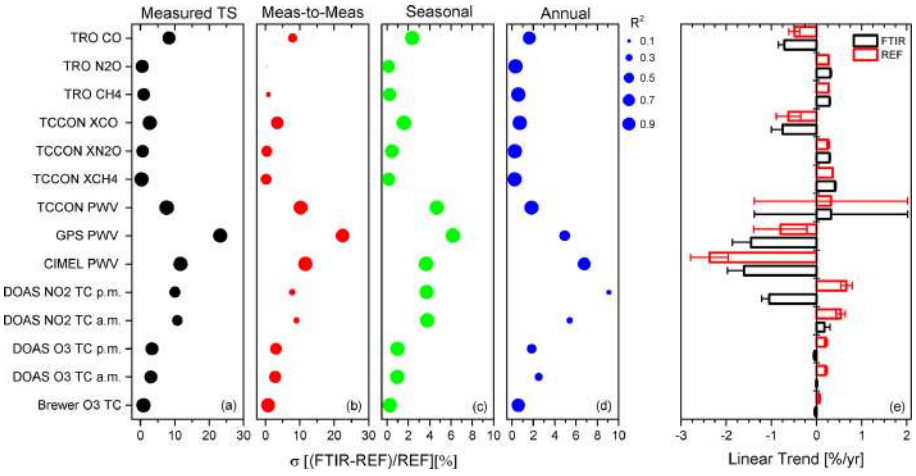

Figure 14. Summary of timescale comparison between FTIR and IZO reference data sets: standard deviation of the relative differences (σ, in %) is displayed on the x axis, and the size of dots represents the determination coefficient, R^2. These statistics are shown for the comparison of **(a)** measured and decomposed time series: **(b)** measurement-to-measurement, **(c)** seasonal, and **(d)** long-term variations (annual means). **(e)** Linear trends (in % yr^{-1}) for coincident FTIR and reference data sets, which are calculated by fitting a linear function combined with a Fourier time series to the data according to Eq. (B1). Errors represent the 95 % confidence interval and were determined using the bootstrap method (see details in Appendix B). Note that TRO refers to the comparison of the tropospheric quantities (GAW in situ records and FTIR VMR averages).

dry bias of sun spectrometers may account for the differences reported among techniques. Regarding the absolute PWV quantification, the NDACC PWV products show a wet bias with respect to all the PWV reference techniques, ranging from ∼ 10 % to ∼ 38 % for TCCON and CIMEL data, respectively. Part of this overestimation is introduced by the NDACC PWV retrievals, ∼ 12 % (Tu et al., 2020), which agrees with the bias obtained with respect to the calibrated TCCON data. The large bias with CIMEL is likely attributed to calibration issues of the standard AERONET CIMEL PWV products. As recently pointed out by Almansa et al. (2020), a dedicated calibration of the CIMEL H_2O channel (centred at 940 nm) at IZO reduces the reported bias by ∼ 20 %.

In relation to PWV seasonality, although the comparability of the different techniques is excellent, the differences among them depend on the PWV values: maximal differences are observed for extreme PWV conditions (i.e. summer and winter months, Fig. 12), which may be due in part to the different seasonal sensitivities of the different measurement techniques. At the longest timescales, the NDACC FTIR, CIMEL, and GPS consistently suggest that PWV values over IZO have been significantly slowing down over the last 2 decades, but the magnitude of this decrease varies among techniques (Fig. 14e). However, the NDACC–TCCON PWV comparison offers contrary results due in part to a more reduced coincident data set (∼ 1100 pairs for NDACC-TCCON versus ∼ 11 000 coincidences for NDACC FTIR–CIMEL–GPS).

4. *Carbon monoxide, methane, and nitrous oxide.* An excellent consistency between the NDACC and TCCON XCO and $X$$CH_4$ records is observed for both the original measured time series and the signals on different timescales. The direct correlation is higher than 0.95 for both gases with a scatter of the relative differences of 0.7 % and 2.7 % for $X$$CH_4$ and XCO, respectively. These values lie within the expected NDACC systematic uncertainty budget (recall Table 3) and the random uncertainty of the TCCON retrievals (Wunch et al., 2015).

   Although the overall comparability of the FTIR $X$$N_2O$ products is satisfactory, it is found to be poorer than the agreement between tropospheric NDACC N_2O and ground-level records. This behaviour can be due to different vertical sensitivities of the NDACC and TCCON products, leading to the NDACC $X$$N_2O$ data being more influenced by the seasonality of the UTLS region, as seen in Fig. 13 and reported by previous studies (García et al., 2014; Zhou et al., 2019). This figure also highlights the remarkable decoupling (even anti-correlation for $X$$CH_4$ and $X$$N_2O$) between the annual cycles of the XGas and tropospheric products. While the seasonality of XGas observations is mostly dominated by the annual shift in the UTLS region, tropospheric concentrations of CO, CH_4, and N_2O are determined by the source emission patterns. As indicated by the comparison to ground-level records, the NDACC tropospheric

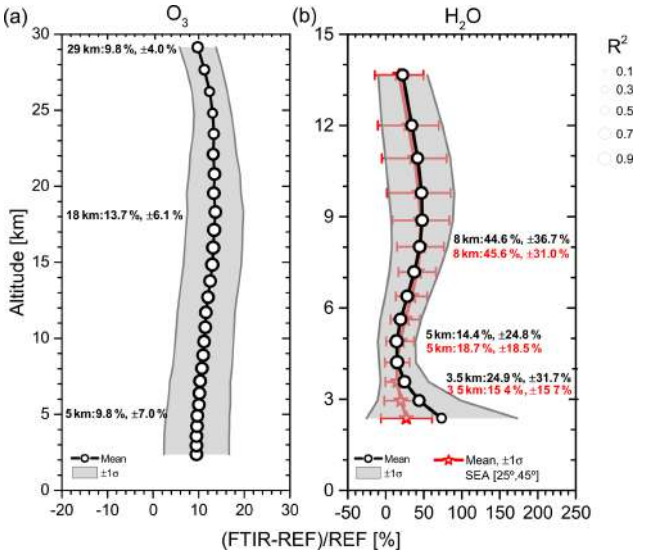

Figure 15. Vertical profile of relative differences between NDACC FTIR VMR profiles and IZO reference data sets (mean and $\pm 1\sigma$ in %) for **(a)** O_3 and **(b)** H_2O. For the latter, the comparison considering only coincidences for FTIR solar elevation angle between 25–45° is also included (in red). The dotted area represents determination coefficient, R^2. Statistics of differences at the altitude levels, well-distinguishable by the FTIR instrument, are included in plots (5, 18, and 29 km for O_3 and 3, 5, and 8 km for H_2O). The number of coincident measurements is 276 in the period 1999–2018 for O_3, and 154 and 32 in the period 2008–2017 for H_2O without and with limiting the FTIR solar zenith angle, respectively.

products properly capture the tropospheric seasonal signals, demonstrating great potential for source–sink attribution studies. The performance of the NDACC tropospheric products can be further improved by means of more sophisticated retrieval strategies, allowing for a reduction of the stratospheric contribution (Sepúlveda et al., 2012, 2014; García et al., 2014). Likewise, the influence of the stratospheric signal on the *X*Gas products can be partially corrected by using co-retrieved *X*HF data or XN_2O (for XCH_4) (Sepúlveda et al., 2012; Wang et al., 2014, and references therein).

In relation to systematic differences, the mean bias is lower than 0.6 % for XCH_4 and XN_2O, indicating no significant spectroscopy inconsistencies between the NIR and MIR spectral regions used for TCCON and NDACC retrievals, respectively. This result is confirmed by comparing the tropospheric NDACC N_2O product to the ground-level records. However, for CH_4, a bias of ~ 2.6 % with respect to surface measurements appears, which is compatible with the assumed error of 3 % in the spectroscopy intensity parameter (Table 3). Concerning CO, the NDACC and TCCON *X*CO products generally differ by ~ 5 %–6 %, which is likely attributed to TCCON post-calibration, as reported by previous works (e.g. Kiel et al., 2016). The TCCON *X*CO calibration factor is 1.0672 ± 0.0200 (recall Sect. 8), which coincides with the bias obtained between the TCCON and NDACC *X*CO products. Note that the comparison with ground-level records points to an underestimation of the NDACC tropospheric CO values (unlike those observed for the TCs), which further emphasizes the presence of a systematic inconsistency.

The timescale analysis was found to be a very useful tool, particularly for tropospheric NDACC comparisons. As illustrated by Fig. 14, the agreement observed between ground-level and tropospheric NDACC products is mainly the result of seasonal and long-term signals. Tropospheric measurement-to-measurement variations, especially for long-lived CH_4 and N_2O gases, are smaller than the FTIR precision and are, therefore, scarcely captured by the remote sensing system (no correlation has been found between FTIR and ground-level observations). Given that CO presents more variable concentrations in the atmosphere, the NDACC FTIR product is able to capture part of its tropospheric variations (correlation of ~ 0.60 on a daily scale).

5. *Water vapour and ozone profiles.* Figure 15 summarizes the comparison between the FTIR O_3 and H_2O VMR profiles and the reference observations (smoothed ECC and humidity sondes). The vertical distribution of differences exhibits different patterns for each gas. For O_3, the difference profile is almost constant until the UTLS region with a mean bias of ~ 10 %–15 % and scatter of ~ 6 %–7 %. Beyond this region, the discrepancies considerably decrease to below ~ 5 % (4.0 % at 29 km) likely due to a better sensitivity of the FTIR system to O_3 variations (recall Fig. 3). Some of the observed discrepancies are introduced by including both FTIR instruments in the comparison. As shown in Sect. 4, the ILS of the IFS 120M spectrometer is noisier and less stable over time than the ILS of IFS 120/5HR, leading to greater uncertainties in the 120M O_3 vertical distribution retrievals. Note that instrumental performance is especially critical for stratospheric gases, like O_3, since the ILS affects the absorption line shape on which the retrieved information is based. When considering only the more stable, well-aligned IFS 120/5HR instrument, García et al. (2021) documented an improvement in comparability between FTIR and ECC sondes by ~ 1 % up to the UTLS and ~ 0.5 % in the middle stratosphere. In addition, as with the total columns, refined FTIR retrieval strategies (i.e. including a simultaneous temperature fit) can further improve the FTIR performance (Schneider et al., 2008a; García et al., 2012, 2021).

On the other hand, the H_2O comparison exhibits a strong vertical stratification with the largest discrepancies located in the lower troposphere (i.e. just above

the island). This pattern is likely due to the substantial impact of the local diurnal up-slope flow on FTIR observations (Schneider et al., 2016). As stated above, diurnal insolation at IZO generates a thermal up-slope flow from the lowermost humid layers, causing a strong H_2O diurnal cycle and thus affecting the H_2O signals measured by the FTIR system (Schneider et al., 2010; González et al., 2016). To examine this effect and ensure the comparison is carried out for free tropospheric conditions, the FTIR observations have also been restricted to low solar elevation angles (between 25 and 45°) (Schneider et al., 2016), with the resulting difference profile also included in Fig. 15 (in red). Despite a considerable decrease in the number of coincidences, this restriction ensures an optimal comparison and that quite similar air masses are detected by both FTIR and meteorological sondes. As a result, the comparability is significantly improved. Until the middle troposphere, both the mean bias and scatter range from 15 %–20 %, while they increase in the upper troposphere (mean bias of 45.6 % and σ of 31.0 % at 8 km). At these altitudes, larger temporal and spatial variability of the humidity fields are expected (Schneider et al., 2016, and references therein), which makes the comparison of the remote sensing and in situ profiles difficult.

For both gases, the scatter values found agree well with the FTIR error estimation (recall Sect. 3.4), with the expected uncertainty for the ECC and meteorological sondes (recall Sect. 8.1), as well as with previous works (Schneider et al., 2008a, 2010, 2016; García et al., 2012, 2021, and references therein). As stated in these studies, although the reference sondes have been smoothed by FTIR averaging kernels, the limited vertical sensitivity of the FTIR profiles could account for part of the dispersion observed between both data sets. Other sources of discrepancies, as mentioned, might be the different observing geometries. Note that the temporal decomposition analysis has not been carried out for profile comparisons given the reduced number of coincidences.

8.4 Influence of sampling

Although the weather conditions at IZO are very favourable for solar measurements, the sampling of FTIR data may not be regular enough and may contain gaps that affect the reliability of the FTIR results, particularly on long-term timescales. In order to examine this effect, Fig. 16 compares the linear trends for coincident FTIR–reference data sets and those computed from the complete reference time series, without pairing to the FTIR observations, in the coincident period shown in Table 4. Note that only those products for which the sampling of the reference data sets is uniform and continuous, have been considered (i.e. GPS PWV observations and ground-level CO, CH_4, and N_2O records). Although some of the other reference techniques have a higher measurement frequency than the FTIR system, they present their own sampling issues (the Brewer and CIMEL data are also biased towards cloud-free days, the DOAS technique measures only during twilight, and the TCCON data have similar sampling to the NDACC FTIR observations). In addition, as in a similar way to Sect. 8.3, the linear trends shown in Fig. 16 have been computed considering individual observations to assess the sampling effects, and they could, therefore, differ from the values presented in Sects. 5 and 6, which are based on FTIR monthly means.

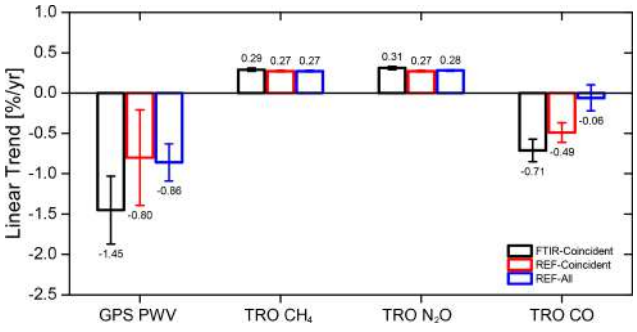

Figure 16. Linear trend (in % yr^{-1}) for coincident FTIR and reference data sets (FTIR–coincident and REF–coincident, respectively) for PWV GPS and ground-level CO, CH_4, and N_2O records. For the reference, the linear trends for the entire time series are also shown, without pairing to FTIR observations, in the coincident period given in Table 4 (REF-All). Trends are calculated by fitting a linear function combined with a Fourier time series to the data according to Eq. (B1) (see details in Appendix B). Trend values are included in the plot for each data set. Error bars represent the 95 % confidence interval.

The overall agreement between the different linear trend estimations is quite high. FTIR sampling has been found to have a minor impact, especially on the stable and long-lived CH_4 and N_2O gases. However, for the more variable CO records, a significant discrepancy is found between considering the entire ground-level time series and those paired with the FTIR observations. This artefact could be, in part, attributed to the sparse FTIR sampling and large dynamical variability in the winter months. As shown in Fig. 13, the greatest differences between FTIR and ground-level data are concentrated in winter, which could induce a bias in the trend values. For PWV, the agreement between the coincident and entire GPS time series demonstrates that the uncertainties induced by FTIR sampling might also be considered negligible. Although there are remarkable differences in the magnitude of the obtained PWV linear trends, they lie within the respective confidence error intervals.

9 Summary and conclusions

Long-term ground-based observations of atmospheric composition are essential to monitor the evolution of the Earth's atmosphere system. Within the NDACC framework, FTIR spectrometry provides abundances of many trace gases simultaneously and with a high degree of precision, which can be used to understand tropospheric and stratospheric chemistry and transport. In this context, the current paper provides an overview of the first 20 years of NDACC FTIR measurements taken at the subtropical Izaña Observatory (IZO, Spain) between 1999 and 2018.

The great potential of the IZO NDACC FTIR records for climate research is internationally recognized, contributing to more than 100 peer-reviewed scientific papers and to numerous international research activities and projects. The major accomplishments drawn from these works are briefly reviewed in the current paper, especially those for investigating the greenhouse gas budgets and long-term changes of pivotal atmospheric gases, or the evaluation of space-based observations and climate model estimations. In addition, a comprehensive assessment of the long-term instrumental performance of the IZO FTIR systems and of the quality and long-term consistency of the different NDACC FTIR products in a coherent manner is presented.

Together with the long-term monitoring of key atmospheric trace gases, analysing the temporal frequency, duration, and extent of the vertical phenomena over IZO (e.g. STE episodes or UTLS vertical movements) could provide useful insights into long-term changes in the dynamics and chemistry of the subtropical atmosphere. Furthermore, the evaluation of possible links to dynamical mechanisms or teleconnection patterns and hemispheric phenomena, such as ENSO (El Niño and the Southern Oscillation), NAO (North Atlantic Oscillation), or QBO (Quasi-Biennial Oscillation), might also serve as tracers of climate change. Dedicated studies using the IZO trace gas time series would be of great use in better understanding these drivers and connections on short-term and long-term scales. The NDACC FTIR multi-decadal data sets, such as those produced by IZO, are therefore indispensable to address the major challenges of current climate research.

Appendix A: NDACC uncertainty budget

The NDACC uncertainty analysis includes the impact of measurement noise and the different model parameter sources. In particular, the error contribution of model parameters can be analytically estimated through the respective error covariance matrix $\mathbf{S}_{x,p}$:

$$\mathbf{S}_{x,p} = \mathbf{G}\mathbf{K}_p\mathbf{S}_p\mathbf{K}_p^{\mathrm{T}}\mathbf{G}^{\mathrm{T}}, \tag{A1}$$

where $\mathbf{S}_p$ is the covariance matrix of the uncertainties $\boldsymbol{\Delta p}$. In this work, $\mathbf{S}_p$ is estimated considering the error sources, values, and partitioning between random and systematic contributions listed in Table A1. They have been identified as the leading error sources and typical values affecting the different FTIR products (Hase, 2007).

The error covariance matrix for measurement noise ($\mathbf{S}_{x,\epsilon}$) is analytically calculated by

$$\mathbf{S}_{x,\epsilon} = \mathbf{G}\mathbf{S}_{y,\epsilon}\mathbf{G}^{\mathrm{T}}, \tag{A2}$$

where $\mathbf{S}_{y,\epsilon}$ is the covariance matrix for noise in the measurement.

The total statistical and systematic uncertainties (listed in Table 3) are then calculated as the square root sum of the squares of all statistical and systematic errors considered, respectively. Note that the measurement noise is considered purely random, while the spectroscopy parameters are purely systematic.

Appendix B: Multi-annual evolution

The multi-annual evolution of the measured time series has been modelled by using a multi-regression fit of different coefficients that consider a mean concentration gas value and variations on different timescales (Sepúlveda et al., 2014; García et al., 2018, and references therein).

$$\begin{aligned} x_m(t) = A_0 + A_1 t + \sum_{1\le i\le N-1} \Bigg\{ & A_{\sin,i} \sin\Big(\frac{2\pi i}{\Delta t} t\Big) \\ & + A_{\cos,i} \cos\Big(\frac{2\pi i}{\Delta t} t\Big)\Bigg\} + \sum_{1\le i\le P} \Bigg\{ B_{\sin,i} \sin\Big(\frac{2\pi i}{\Delta j} j(t)\Big) \\ & + B_{\cos,i} \cos\Big(\frac{2\pi i}{\Delta j} j(t)\Big)\Bigg\} \end{aligned} \tag{B1}$$

Coefficients A_i capture the long-term variations: A_0 and A_1 are related to the linear changes, while coefficients $A_{\sin,i}$ and $A_{\cos,i}$ define the amplitude and phases of a Fourier series that considers all frequencies between 1 and $N-1$. Here N is the total number of years covered by the whole time series, and $\Delta t = \max\{t\} - \min\{t\}$ is the time period covered by the whole time series. The coefficients $B_{\sin,i}$ and $B_{\cos,i}$ capture the intra-annual variation (season cycle) by fitting amplitude and phases of a Fourier series that considers all frequencies between 1 and p. We consider frequencies up to two per year ($P = 2$) and $\Delta j = \max\{j(t)\} - \min\{j(t)\}$ as the intra-annual Julian day period covered by the data and $j(t)$ the intra-annual Julian day (intra-annual Julian day means Julian day starting each year with 0; i.e, $j(t)$ is between 0 and 366). Note that $N = \frac{\Delta t}{\Delta j}$.

The uncertainty ranges of the fit parameters, including the linear trends, is calculated using the bootstrap resampling method (García et al., 2012, 2021, and references therein). This approach is based on recurrently estimating the fit parameters on a modified time series, which results from randomly disturbing the original time series with the residues between the multi-regression fit and the original time series.

Table A1. List of sources and values used for the uncertainty analysis. (MEA: modulation efficiency amplitude; ν scale: spectral position; S: intensity; γ: pressure broadening parameter). The third column provides the partitioning of the error values between statistical (ST) and systematic (SY) contributions.

Uncertainty source	Uncertainty value	ST/SY
Baseline (channelling and offset)	0.2 and 0.1 %	50/50
ILS (MEA and phase error)	1 % and 0.01 rad	50/50
Pointing offset	0.1°	90/10
Solar lines (intensity and ν scale)	1 % and 10^{-6}	80/20
Temperature profile (2.37–10, 11–36, 37–120 km)	1, 2, 5 K	70/30
Spectroscopy γ	5 %	0/100
Spectroscopy S for CO, $H_2^{16}O$, $H_2^{18}O$, $HD^{16}O$, N_2O, OCS	2 %	0/100
Spectroscopy S for CH_4	3 %	0/100
Spectroscopy S for C_2H_6, HF, HCl, NO, O_3	5 %	0/100
Spectroscopy S for $ClONO_2$, HCN, H_2CO, HNO_3, NO_2	10 %	0/100

Thereby, it does not assume that residues follow any specific distribution (i.e. Gaussian) and are uniform over time, which could occur if the modelled fit is not able to properly capture the measured time series.

This multi-regression fit has also been used to temporally decompose the FTIR and reference time series, when the quality assessment of the FTIR products is addressed (Sect. 8). For the hourly and daily mean comparison (so-called measurement-to-measurement comparison), we work with the de-seasonalized and de-trended time series in order to ensure that the comparison between the measured inter-day variabilities is not affected by the seasonal and long-term signals. This time series is calculated by subtracting from the measured time series (reference or FTIR) the corresponding linear trend and inter-annual and intra-annual signals obtained from the multi-regression fit. For the seasonal comparison, an averaged annual cycle is computed from the multi-annual averaged monthly means of the de-trended time series (measured time series minus the linear trend and the inter-annual variations). Finally, the long-term signals given by the annual means are computed from the de-seasonalized time series, which is computed by subtracting the intra-annual variations from the measured time series. Note that to obtain the linear trends in percentage, the measured time series is transformed on a logarithmic scale. Since the trace gas short-term variations are usually much smaller than the climatological or long-term background values, the variations on the logarithmic scale can be interpreted as the variations relative to the long-term background reference.

Data availability. The NDACC FTIR and DOAS products, as well as the ozone sondes, are available from the NDACC archive (http://www.ndaccdemo.org, NDACC, 2021). The TCCON FTIR data are accessible via the TCCON Data Archive, hosted by CaltechDATA (https://doi.org/10.14291/TCCON.GGG2014.IZANA01.R1, Blumenstock et al., 2017). The CIMEL PWV data can be downloaded from the AERONET database (https://aeronet.gsfc.nasa.gov/, NASA, 2021), while the water vapour sondes are available from the GRUAN archive (https://www.gruan.org, GCOS, 2021). The Brewer ozone and GPS PWV data are available by request from the corresponding authors. The ground-level greenhouse and carbon cycle gases are archived in the World Data Centre for Greenhouse Gases (WDCGG) under the WMO-GAW programme (https://gaw.kishou.go.jp/, WDCGG, 2021).

Author contributions. OEG and MS designed and wrote the structure and methodology of the paper and computed the calculations required. FH, TB, JG, SB, and ANR discussed the results and provided the NDACC and TCCON retrievals. EC and TB ensured the provision of funds for the IZO FTIR measurement programme. OEG, MS, ESe, ESa, CL, and YG performed the maintenance and quality control of the FTIR measurements. RR, AJGP, ER, PPR, and RDG are responsible for the maintenance, quality-control, and data generation of the WMO-GAW greenhouse gases programme at IZO. MNC, OP, and MY are in charge of the NDACC DOAS observations at IZO. AR, VC, and SFLL are responsible for the maintenance of RBCC-E Brewer spectrometers as well as for providing the NDACC Brewer ozone observations. PMRC and MH are responsible for the PWV data and GRUAN humidity profiles, respectively. CT and NP are in charge of the ozonesonde programme at IZO. Finally, all authors discussed the results and contributed to the final paper.

Competing interests. The authors declare that they have no conflict of interest.

Disclaimer. Publisher's note: Copernicus Publications remains neutral with regard to jurisdictional claims in published maps and institutional affiliations.

Acknowledgements. This work has been developed within the framework of the activities of the World Meteorological Organization (WMO) Commission for Instruments and Methods of Obser-

vation (CIMO) Izaña test bed for aerosols and water vapour remote sensing instruments.

Financial support. The Izaña FTIR station has been supported by the German Bundesministerium für Wirtschaft und Energie (BMWi) via DLRunder grants 50EE1711A and by the Helmholtz Association via the research programme ATMO. In addition, this research was funded by the European Research Council under FP7/(2007–2013)/ERC grant agreement no. 256961 (project MUSICA), by the Deutsche Forschungsgemeinschaft for the project MOTIV (GeschaFTIRzeichen SCHN 1126/2-1), by the Ministerio de Economía y Competitividad from Spain through the projects CGL2012-37505 (project NOVIA) and CGL2016-80688-P (project INMENSE), and by EUMETSAT under its Fellowship Programme (project VALIASI).

Review statement. This paper was edited by Stelios Kazadzis and reviewed by three anonymous referees.

References

Almansa, A., Cuevas, E., Barreto, Á., Torres, B., García, O., García, R., Velasco-Merino, C., Cachorro, V., Berjón, A., Mallorquín, M., López, C., Ramos, R., Guirado-Fuentes, C., Negrillo, R., and de Frutos, Á. M.: Column Integrated Water Vapor and Aerosol Load Characterization with the New ZEN-R52 Radiometer, Remote Sensing, 12, 1424, https://doi.org/10.3390/rs12091424, 2020.

Bader, W., Bovy, B., Conway, S., Strong, K., Smale, D., Turner, A. J., Blumenstock, T., Boone, C., Collaud Coen, M., Coulon, A., Garcia, O., Griffith, D. W. T., Hase, F., Hausmann, P., Jones, N., Krummel, P., Murata, I., Morino, I., Nakajima, H., O'Doherty, S., Paton-Walsh, C., Robinson, J., Sandrin, R., Schneider, M., Servais, C., Sussmann, R., and Mahieu, E.: The recent increase of atmospheric methane from 10 years of ground-based NDACC FTIR observations since 2005, Atmos. Chem. Phys., 17, 2255–2277, https://doi.org/10.5194/acp-17-2255-2017, 2017.

Barthlott, S., Schneider, M., Hase, F., Wiegele, A., Christner, E., González, Y., Blumenstock, T., Dohe, S., García, O. E., Sepúlveda, E., Strong, K., Mendonca, J., Weaver, D., Palm, M., Deutscher, N. M., Warneke, T., Notholt, J., Lejeune, B., Mahieu, E., Jones, N., Griffith, D. W. T., Velazco, V. A., Smale, D., Robinson, J., Kivi, R., Heikkinen, P., and Raffalski, U.: Using XCO_2 retrievals for assessing the long-term consistency of NDACC/FTIR data sets, Atmos. Meas. Tech., 8, 1555–1573, https://doi.org/10.5194/amt-8-1555-2015, 2015.

Barthlott, S., Schneider, M., Hase, F., Blumenstock, T., Kiel, M., Dubravica, D., García, O. E., Sepúlveda, E., Mengistu Tsidu, G., Takele Kenea, S., Grutter, M., Plaza-Medina, E. F., Stremme, W., Strong, K., Weaver, D., Palm, M., Warneke, T., Notholt, J., Mahieu, E., Servais, C., Jones, N., Griffith, D. W. T., Smale, D., and Robinson, J.: Tropospheric water vapour isotopologue data (H216O, H218O, and HD16O) as obtained from NDACC/FTIR solar absorption spectra, Earth Syst. Sci. Data, 9, 15–29, https://doi.org/10.5194/essd-9-15-2017, 2017.

Birk, M. and Wagner, G.: A new spectroscopic database for chlorine nitrate, in: 6th Biennial HITRAN Conference, Cambridge, USA, 2000.

Blumenstock, T., Kohlhepp, R., Barthlott, S., E.García, O., Hase, F., Kiefer, M., Raffalski, U., and Schneider, M.: Investigation of long-term Stability of MIPAS-ENVISAT O_3 and HNO_3 Data using ground-based FTIR Measurements in Kiruna (S) and Izaña (E), in: ACVE Conference 2013, Frascati, Italia, 2013.

Blumenstock, T., Hase, F., Schneider, M., García, O. E., and Sepúlveda, E.: TCCON data from Izana (ES), Release GGG2014.R1, Version R1, CaltechDATA [data set], https://doi.org/10.14291/TCCON.GGG2014.IZANA01.R1, 2017.

Borger, C., Schneider, M., Ertl, B., Hase, F., García, O. E., Sommer, M., Höpfner, M., Tjemkes, S. A., and Calbet, X.: Evaluation of MUSICA IASI tropospheric water vapour profiles using theoretical error assessments and comparisons to GRUAN Vaisala RS92 measurements, Atmos. Meas. Tech., 11, 4981–5006, https://doi.org/10.5194/amt-11-4981-2018, 2018.

Borsdorff, T., aan de Brugh, J., Hu, H., Hasekamp, O., Sussmann, R., Rettinger, M., Hase, F., Gross, J., Schneider, M., Garcia, O., Stremme, W., Grutter, M., Feist, D. G., Arnold, S. G., De Mazière, M., Kumar Sha, M., Pollard, D. F., Kiel, M., Roehl, C., Wennberg, P. O., Toon, G. C., and Landgraf, J.: Mapping carbon monoxide pollution from space down to city scales with daily global coverage, Atmos. Meas. Tech., 11, 5507–5518, https://doi.org/10.5194/amt-11-5507-2018, 2018.

Cuevas, E., González, Y., Rodríguez, S., Guerra, J. C., Gómez-Peláez, A. J., Alonso-Pérez, S., Bustos, J., and Milford, C.: Assessment of atmospheric processes driving ozone variations in the subtropical North Atlantic free troposphere, Atmos. Chem. Phys., 13, 1973–1998, https://doi.org/10.5194/acp-13-1973-2013, 2013.

Cuevas, E., Milford, C., Bustos, J. J. R., García, O. E., García, R. D., Gómez-Peláez, A. J., Guirado-Fuentes, C., Marrero, C., Prats, N., Ramos, R., Redondas, A., Reyes, E., Rivas-Soriano, P. P., Rodríguez, S., Romero-Campos, P. M., Torres, C. J., Schneider, M., Yela, M., Belmonte, J., del Campo-Hernández, R., Almansa, F., Barreto, A., López-Solano, C., Basart, S., Terradellas, E., Werner, E., Afonso, S., Bayo, C., Berjón, A., Carreño, V., Castro, N. J., Chinea, N., Cruz, A. M., Damas, M., De Ory-Ajamil, F., García, M., Gómez-Trueba, V., Hernández, C., Hernández, Y., Hernández-Cruz, B., León-Luís, S. F., López-Fernández, R., López-Solano, J., Parra, F., Rodríguez, E., Rodríguez-Valido, M., Sálamo, C., Sanromá, E., Santana, D., Santo Tomás, F., Sepúlveda, E., and Sosa, E.: Izaña Atmospheric Research Center Activity Report 2017–2018, edited by: Cuevas, E., Milford, C., and Tarasova, O., State Meteorological Agency (AEMET), Madrid, Spain, and World Meteorological Organization (WMO), Geneva, Switzerland, WMO/GAW Report No. 247, 2019.

De Mazière, M., Thompson, A. M., Kurylo, M. J., Wild, J. D., Bernhard, G., Blumenstock, T., Braathen, G. O., Hannigan, J. W., Lambert, J.-C., Leblanc, T., McGee, T. J., Nedoluha, G., Petropavlovskikh, I., Seckmeyer, G., Simon, P. C., Steinbrecht, W., and Strahan, S. E.: The Network for the Detection of Atmospheric Composition Change (NDACC): history, status and perspectives, Atmos. Chem. Phys., 18, 4935–4964, https://doi.org/10.5194/acp-18-4935-2018, 2018.

Dubravica, D., Birk, M., Hase, F., Loos, J., Palm, M., Sadeghi, A., and Wagner, G.: Improved spectroscopic parameters of methane in the MIR for atmospheric remote sensing, in: High Resolution Molecular Spectroscopy 2013 meeting, available at: http://lmsd.chem.elte.hu/hrms/abstracts/D16.pdf (last access: 1 April 2021), 2013.

Franco, B., Mahieu, E., Emmons, L. K., Tzompa-Sosa, Z. A., Fischer, E. V., Sudo, K., Bovy, B., Conway, S., Griffin, D., Hannigan, J. W., Strong, K., and Walker, K. A.: Evaluating ethane and methane emissions associated with the development of oil and natural gas extraction in North America, Environ. Res. Lett., 11, 044010, https://doi.org/10.1088/1748-9326/11/4/044010, 2016.

Frey, M., Sha, M. K., Hase, F., Kiel, M., Blumenstock, T., Harig, R., Surawicz, G., Deutscher, N. M., Shiomi, K., Franklin, J. E., Bösch, H., Chen, J., Grutter, M., Ohyama, H., Sun, Y., Butz, A., Mengistu Tsidu, G., Ene, D., Wunch, D., Cao, Z., Garcia, O., Ramonet, M., Vogel, F., and Orphal, J.: Building the COllaborative Carbon Column Observing Network (COCCON): long-term stability and ensemble performance of the EM27/SUN Fourier transform spectrometer, Atmos. Meas. Tech., 12, 1513–1530, https://doi.org/10.5194/amt-12-1513-2019, 2019.

García, M. I., van Drooge, B. L., Rodríguez, S., and Alastuey, A.: Speciation of organic aerosols in the Saharan Air Layer and in the free troposphere westerlies, Atmos. Chem. Phys., 17, 8939–8958, https://doi.org/10.5194/acp-17-8939-2017, 2017.

García, O. E., Schneider, M., Redondas, A., González, Y., Hase, F., Blumenstock, T., and Sepúlveda, E.: Investigating the long-term evolution of subtropical ozone profiles applying ground-based FTIR spectrometry, Atmos. Meas. Tech., 5, 2917–2931, https://doi.org/10.5194/amt-5-2917-2012, 2012.

García, O. E., Sepúlveda, E., Schneider, M., Hase, F., August, T., Blumenstock, T., Kühl, S., Munro, R., Gómez-Peláez, Á. J., Hultberg, T., Redondas, A., Barthlott, S., Wiegele, A., González, Y., and Sanromá, E.: Consistency and quality assessment of the Metop-A/IASI and Metop-B/IASI operational trace gas products (O_3, CO, N_2O, CH_4, and CO_2) in the subtropical North Atlantic, Atmos. Meas. Tech., 9, 2315–2333, https://doi.org/10.5194/amt-9-2315-2016, 2016.

García, O. E., Schneider, M., Ertl, B., Sepúlveda, E., Borger, C., Diekmann, C., Wiegele, A., Hase, F., Barthlott, S., Blumenstock, T., Raffalski, U., Gómez-Peláez, A., Steinbacher, M., Ries, L., and de Frutos, A. M.: The MUSICA IASI CH4 and N2O products and their comparison to HIPPO, GAW and NDACC FTIR references, Atmos. Meas. Tech., 11, 4171–4215, https://doi.org/10.5194/amt-11-4171-2018, 2018.

García, O. E., Sanromá, E., Schneider, M., Hase, F., León-Luis, S. F., Blumenstock, T., Sepúlveda, E., Redondas, A., Carreño, V., Torres, C., and Prats, N.: Improved ozone monitoring by ground-based FTIR spectrometry, Atmos. Meas. Tech. Discuss. [preprint], https://doi.org/10.5194/amt-2021-67, in review, 2021.

García, O. E., Schneider, M., Hase, F., Blumenstock, T., Sepúlveda, E., Gómez-Peláez, A., Barthlott, S., Dohe, S., González, Y., Meinhardt, F., and Steinbacher, M.: Monitoring of N2O by ground-based FTIR: optimisation of retrieval strategies and comparison to GAW insitu observations, in: NDACC-IRWG/TCCON meeting 2014, Bad Sulza, Germany, 2014.

Gaudel, A., Cooper, O., Ancellet, G., Barret, B., Boynard, A., Burrows, J., Clerbaux, C., Coheur, P.-F., Cuesta, J.and Cuevas, E., Doniki, S., Dufour, G., Ebojie, F., Foret, G., García, O., Granados Muños, M., Hannigan, J., Hase, F., Huang, G., Hassler, B., Hurtmans, D., Jaffe, D., Jones, N., Kalabokas, P., Kerridge, B., Kulawik, S., Latter, B., Leblanc, T., Le FlochmoÃ«n, E., Lin, W., Liu, J., Liu, X., Mahieu, E., McClure-Begley, A., Neu, J., Osman, M., Palm, M., Petetin, H., Petropavlovskikh, I., Querel, R., Rahpoe, N., Rozanov, A., Schultz, M., Schwab, J., Siddans, R., Smale, D., Steinbacher, M., Tanimoto, H., Tarasick, D., Thouret, V., Thompson, A., Trickl, T., Weatherhead, E., Wespes, C., Worden, H., Vigouroux, C., Xu, X., Zeng, G., and Ziemke, J.: Tropospheric Ozone Assessment Report: Present-day distribution and trends of tropospheric ozone relevant to climate and global atmospheric chemistry model evaluation, Elementa, 6, 39, https://doi.org/10.1525/elementa.291, 2018.

GCOS: GRUAN archive, available at: https://www.gruan.org, last access: 1 April 2021.

Gil-Ojeda, M., Navarro-Comas, M., Redondas, A., Puentedura, O., Hendrick, F., van Roozendael, M., Iglesias, J., and Cuevas, E.: Total ozone measurements from the NDACC Izaña Subtropical Station: Visible spectroscopy versus Brewer and satellite instruments, in: Quadrennial Ozone Symposium 2012 (QOS 2012), vol. ID:6064, Toronto, Canada, 2012.

Gisi, M., Hase, F., Dohe, S., and Blumenstock, T.: Camtracker: a new camera controlled high precision solar tracker system for FTIR-spectrometers, Atmos. Meas. Tech., 4, 47–54, https://doi.org/10.5194/amt-4-47-2011, 2011.

Goldman, A., Tipping, R., Ma, Q., Boone, C., Bernath, P., Demoulin, P., Hase, F., Schneider, M., Hannigan, J., Coffey, M., and Rinsland, C.: On the line parameters for the $X^1\sum_g^+(1\text{–}0)$ infrared quadrupolar transitions of $^{14}N_2$, J. Quant. Spectrosc. Ra., 103, 168–174, https://doi.org/10.1016/j.jqsrt.2006.05.010, 2007.

González, Y., Schneider, M., Dyroff, C., Rodríguez, S., Christner, E., García, O. E., Cuevas, E., Bustos, J. J., Ramos, R., Guirado-Fuentes, C., Barthlott, S., Wiegele, A., and Sepúlveda, E.: Detecting moisture transport pathways to the subtropical North Atlantic free troposphere using paired H_2O-δD in situ measurements, Atmos. Chem. Phys., 16, 4251–4269, https://doi.org/10.5194/acp-16-4251-2016, 2016.

Gottwald, M., Bovensmann, H., Lichtenberg, G., Noel, S., von Bargen, A., Slijkhuis, S., Piters, A., Hoogeveen, R., von Savigny, C., Buchwitz, M., Kokhanovsky, A., Richter, A., Rozanov, A., Holzzer-Popp, T., Bramstedt, K., Lambert, J.-C., Skupin, J., Wittrock, F., Schrijver, H., and Burrows, J.: SCIAMACHY, Monitoring the Cahnging Earth's Atmosphere, Tech. rep., Germany, 2006.

Griffiths, P. R. and de Haseth, J. A.: Fourier Transform Infrared Spectrometry, John Wiley & Sons, Inc, New Jersey, USA, 2007.

Gröbner, J., Redondas, A., Weber, M., and Bais, A.: Final report of the project Traceability for atmospheric total column ozone (ENV59, ATMOZ), Tech. rep., EURAMET, available at: https://www.euramet.org/research-innovation/search-research-projects/details/project/traceability-for-atmospheric-total-column-ozone/ (last access: 1 April 2021), 2017.

Harrison, J., Allen, N., and Bernath, P.: Infrared absorption cross sections for ethane (C_2H_6) in the 3 µm region, J. Quant. Spectrosc. Ra., 111, 357–363, https://doi.org/10.1016/j.jqsrt.2009.09.010, 2010.

Hase, F.: Inversion von Spurengasprofilen aus hochaufgelösten bodengebundenen FTIR-Messungen in Absorption, Tech. rep., Forschungszentrum Karlsruhe, Germany, 2000.

Hase, F.: Error Estimation in PROFFIT revisited, in: NDSC IRWG Meeting, Tenerife, Spain, 2007.

Hase, F.: Improved instrumental line shape monitoring for the ground-based, high-resolution FTIR spectrometers of the Network for the Detection of Atmospheric Composition Change, Atmos. Meas. Tech., 5, 603–610, https://doi.org/10.5194/amt-5-603-2012, 2012.

Hase, F., Hanningan, J. W., Coffey, M. T., Goldman, A., Höfner, M., Jones, N. B., Rinsland, C. P., and Wood, S. W.: Intercomparison of retrieval codes used for the analysis of high-resolution ground-based FTIR measurements, J. Quant. Spectrosc. Ra., 87, 25–52, 2004.

Hase, F., Blumenstock, T., Schneider, M., and Sepulveda, E.: Interactive comment on "Strategy for high-accuracy-and-precision retrieval of atmospheric methane from the mid-infrared FTIR network" by R. Sussmann et al., Atmos. Meas. Tech. Discuss., 4, C1048–C1048, available at: https://www.atmos-meas-tech-discuss.net/4/C1048/2011/ (last access: 1 April 2021), 2011.

Heffernan, O.: The mystery of the expanding tropics, Nature, 530, 20–22, https://doi.org/10.1038/530020a, 2016.

Hegglin, M. I. and Shepherd, T. G.: Large climate-induced changes in ultraviolet index and stratosphere-to-troposphere ozone flux, Nat. Geosci., 2, 687–691, https://doi.org/10.1038/NGEO604, 2009.

Höpfner, M., von Clarmann, T., Fischer, H., Funke, B., Glatthor, N., Grabowski, U., Kellmann, S., Kiefer, M., Linden, A., Milz, M., Steck, T., Stiller, G. P., Bernath, P., Blom, C. E., Blumenstock, Th., Boone, C., Chance, K., Coffey, M. T., Friedl-Vallon, F., Griffith, D., Hannigan, J. W., Hase, F., Jones, N., Jucks, K. W., Keim, C., Kleinert, A., Kouker, W., Liu, G. Y., Mahieu, E., Mellqvist, J., Mikuteit, S., Notholt, J., Oelhaf, H., Piesch, C., Reddmann, T., Ruhnke, R., Schneider, M., Strandberg, A., Toon, G., Walker, K. A., Warneke, T., Wetzel, G., Wood, S., and Zander, R.: Validation of MIPAS ClONO2 measurements, Atmos. Chem. Phys., 7, 257–281, https://doi.org/10.5194/acp-7-257-2007, 2007.

IRWG: Infrared Working Group Uniform Retrieval Parameter Summary, Tech. rep., available at: http://www.acom.ucar.edu/irwg/IRWG_Uniform_RP_Summary-3.pdf (last access: 1 April 2021), 2014.

Kiel, M., Hase, F., Blumenstock, T., and Kirner, O.: Comparison of XCO abundances from the Total Carbon Column Observing Network and the Network for the Detection of Atmospheric Composition Change measured in Karlsruhe, Atmos. Meas. Tech., 9, 2223–2239, https://doi.org/10.5194/amt-9-2223-2016, 2016.

Kohlhepp, R., Ruhnke, R., Chipperfield, M. P., De Mazière, M., Notholt, J., Barthlott, S., Batchelor, R. L., Blatherwick, R. D., Blumenstock, Th., Coffey, M. T., Demoulin, P., Fast, H., Feng, W., Goldman, A., Griffith, D. W. T., Hamann, K., Hannigan, J. W., Hase, F., Jones, N. B., Kagawa, A., Kaiser, I., Kasai, Y., Kirner, O., Kouker, W., Lindenmaier, R., Mahieu, E., Mittermeier, R. L., Monge-Sanz, B., Morino, I., Murata, I., Nakajima, H., Palm, M., Paton-Walsh, C., Raffalski, U., Reddmann, Th., Rettinger, M., Rinsland, C. P., Rozanov, E., Schneider, M., Senten, C., Servais, C., Sinnhuber, B.-M., Smale, D., Strong, K., Sussmann, R., Taylor, J. R., Vanhaelewyn, G., Warneke, T., Whaley, C., Wiehle, M., and Wood, S. W.: Observed and simulated time evolution of HCl, $ClONO_2$, and HF total column abundances, Atmos. Chem. Phys., 12, 3527–3556, https://doi.org/10.5194/acp-12-3527-2012, 2012.

Lejeune, B., Mahieu, E., Vollmer, M. K., Reimann, S., Bernath, P. F., Boone, C. D., Walker, K. A., and Servais, C.: Optimized approach to retrieve information on atmospheric carbonyl sulfide (OCS) above the Jungfraujoch station and change in its abundance since 1995, J. Quant. Spectrosc. Ra., 186, 81–95, https://doi.org/10.1016/j.jqsrt.2016.06.001, 2016.

Mahieu, E., Chipperfield, M., Notholt, J., Reddmann, T., Anderson, J., Bernath, P., Blumenstock, T., Coffey, M., Dhomse, S., Feng, W., Franco, B., Froidevaux, L., Griffith, D., Hannigan, J., Hase, F., Hossaini, R., Jones, N., Morino, I., Murata, I., Nakajima, H., Palm, M., Paton-Walsh, C., Russell, J., Schneider, M., Servais, C., Smale, D., and Walker, K.: Recent Northern Hemisphere stratospheric HCl increase due to atmospheric circulation changes, Nature, 515, 104–107, https://doi.org/10.1038/nature13857, 2014.

Mahieu, E., Franco, B., Pozzer, A., Taraborrelli, D., Bader, W., Prignon, M., and Servais, C.: Observation and simulation of ethane at 23 FTIR sites, in: Proceeding from the 20th EGU General Assembly, vol. 2018EGUGA..2013950M, p. 13950, Vienna, Austria, 2018.

Masson-Delmotte, V., Zhai, P., Pirani, A., Connors, S. L., Péan, C., Berger, S., Caud, N., Chen, Y., Goldfarb, L., Gomis, M. I., Huang, M., Leitzell, K., Lonnoy, E., Matthews, J. B. R., Maycock, T. K., Waterfield, T., Yelekçi, O., Yu, R., and Zhou, B. (Eds.): Climate Change 2021: The Physical Science Basis. Contribution of Working Group I to the Sixth Assessment Report of the Intergovernmental Panel on Climate Change, Tech. rep., Cambridge University Press, in press, 2021.

NASA: AERONET database, available at: https://aeronet.gsfc.nasa.gov/, last access: 1 April 2021.

NDACC: NDACC archive, available at: http://www.ndaccdemo.org, last access: 1 April 2021.

Rinsland, C. P., Weisenstein, D. K., Ko, M. K. W., Scott, C. J., Chiou, L. S., Mahieu, E., Zander, R., and Demoulin, P.: Post-Mount Pinatubo eruption ground-based infrared stratospheric column measurements of HNO_3, NO, and NO_2 and their comparison with model calculations, J. Geophys. Res., 108, 4437, https://doi.org/10.1029/2002JD002965, 2003.

Risi, C., Noone, D., Worden, J., Frankenberg, C., Stiller, G., Kiefer, M., Funke, B., Walker, K., Bernath, P., Schneider, M., Wunch, D., Sherlock, V., Deutscher, N., Griffith, D., Wennberg, P., Strong, K., Smale, D., Mahieu, E., Barthlott, S., Hase, F., García, O., Notholt, J., Warneke, T., Toon, G., Sayres, D., Bony, S., Lee, J., Brown, D., Uemura, R., and Sturm, C.: Process-evaluation of tropospheric humidity simulated by general circulation models using water vapor isotopologues: 1. Comparison between models and observations, J. Geophys. Res., 117, D05303, https://doi.org/10.1029/2011JD016621, 2012.

Robles-Gonzalez, C., Navarro-Comas, M., Puentedura, O., Schneider, M., Hase, F., Garcia, O., Blumenstock, T., and Gil-Ojeda, M.: Intercomparison of stratospheric nitrogen dioxide columns retrieved from ground-based DOAS and FTIR and satellite DOAS instruments over the subtropical Izana station, Atmos. Meas. Tech., 9, 4471–4485, https://doi.org/10.5194/amt-9-4471-2016, 2016.

Rodgers, C.: Inverse Methods for Atmospheric Sounding: Theory and Praxis, World Scientific Publishing Co., Singapore, 2000.

Scheepmaker, R. A., Frankenberg, C., Deutscher, N. M., Schneider, M., Barthlott, S., Blumenstock, T., Garcia, O. E., Hase, F., Jones, N., Mahieu, E., Notholt, J., Velazco, V., Landgraf, J., and Aben, I.: Validation of SCIAMACHY HDO/H_2O measurements using the TCCON and NDACC-MUSICA networks, Atmos. Meas. Tech., 8, 1799–1818, https://doi.org/10.5194/amt-8-1799-2015, 2015.

Schneider, M., Blumenstock, T., Chipperfield, M. P., Hase, F., Kouker, W., Reddmann, T., Ruhnke, R., Cuevas, E., and Fischer, H.: Subtropical trace gas profiles determined by ground-based FTIR spectroscopy at Izaña (28° N, 16° W): Five-year record, error analysis, and comparison with 3-D CTMs, Atmos. Chem. Phys., 5, 153–167, https://doi.org/10.5194/acp-5-153-2005, 2005.

Schneider, M., Hase, F., Blumenstock, T., Redondas, A., and Cuevas, E.: Quality assessment of O_3 profiles measured by a state-of-the-art ground-based FTIR observing system, Atmos. Chem. Phys., 8, 5579–5588, https://doi.org/10.5194/acp-8-5579-2008, 2008a.

Schneider, M., Redondas, A., Hase, F., Guirado, C., Blumenstock, T., and Cuevas, E.: Comparison of ground-based Brewer and FTIR total column O_3 monitoring techniques, Atmos. Chem. Phys., 8, 5535–5550, https://doi.org/10.5194/acp-8-5535-2008, 2008b.

Schneider, M., Romero, P. M., Hase, F., Blumenstock, T., Cuevas, E., and Ramos, R.: Continuous quality assessment of atmospheric water vapour measurement techniques: FTIR, Cimel, MFRSR, GPS, and Vaisala RS92, Atmos. Meas. Tech., 3, 323–338, https://doi.org/10.5194/amt-3-323-2010, 2010.

Schneider, M., Barthlott, S., Hase, F., González, Y., Yoshimura, K., García, O. E., Sepúlveda, E., Gomez-Pelaez, A., Gisi, M., Kohlhepp, R., Dohe, S., Blumenstock, T., Wiegele, A., Christner, E., Strong, K., Weaver, D., Palm, M., Deutscher, N. M., Warneke, T., Notholt, J., Lejeune, B., Demoulin, P., Jones, N., Griffith, D. W. T., Smale, D., and Robinson, J.: Ground-based remote sensing of tropospheric water vapour isotopologues within the project MUSICA, Atmos. Meas. Tech., 5, 3007–3027, https://doi.org/10.5194/amt-5-3007-2012, 2012.

Schneider, M., Wiegele, A., Barthlott, S., González, Y., Christner, E., Dyroff, C., García, O. E., Hase, F., Blumenstock, T., Sepúlveda, E., Mengistu Tsidu, G., Takele Kenea, S., Rodríguez, S., and Andrey, J.: Accomplishments of the MUSICA project to provide accurate, long-term, global and high-resolution observations of tropospheric H2O,δD pairs – a review, Atmos. Meas. Tech., 9, 2845–2875, https://doi.org/10.5194/amt-9-2845-2016, 2016.

Seidel, D., Fu, Q., Randel, W., and Reichler, T.: Widening of the tropical belt in a changing climate, Nat. Geosci., 1, 21–24, https://doi.org/10.1038/ngeo.2007.38, 2008.

Sepúlveda, E., Schneider, M., Hase, F., García, O. E., Gomez-Pelaez, A., Dohe, S., Blumenstock, T., and Guerra, J. C.: Long-term validation of tropospheric column-averaged CH4 mole fractions obtained by mid-infrared ground-based FTIR spectrometry, Atmos. Meas. Tech., 5, 1425–1441, https://doi.org/10.5194/amt-5-1425-2012, 2012.

Sepúlveda, E., Schneider, M., Hase, F., Barthlott, S., Dubravica, D., García, O. E., Gomez-Pelaez, A., González, Y., Guerra, J. C., Gisi, M., Kohlhepp, R., Dohe, S., Blumenstock, T., Strong, K., Weaver, D., Palm, M., Sadeghi, A., Deutscher, N. M., Warneke, T., Notholt, J., Jones, N., Griffith, D. W. T., Smale, D., Brailsford, G. W., Robinson, J., Meinhardt, F., Steinbacher, M., Aalto, T., and Worthy, D.: Tropospheric CH_4 signals as observed by NDACC FTIR at globally distributed sites and comparison to GAW surface in situ measurements, Atmos. Meas. Tech., 7, 2337–2360, https://doi.org/10.5194/amt-7-2337-2014, 2014.

Sha, M. K., Langerock, B., Blavier, J.-F. L., Blumenstock, T., Borsdorff, T., Buschmann, M., Dehn, A., De Mazière, M., Deutscher, N. M., Feist, D. G., García, O. E., Griffith, D. W. T., Grutter, M., Hannigan, J. W., Hase, F., Heikkinen, P., Hermans, C., Iraci, L. T., Jeseck, P., Jones, N., Kivi, R., Kumps, N., Landgraf, J., Lorente, A., Mahieu, E., Makarova, M. V., Mellqvist, J., Metzger, J.-M., Morino, I., Nagahama, T., Notholt, J., Ohyama, H., Ortega, I., Palm, M., Petri, C., Pollard, D. F., Rettinger, M., Robinson, J., Roche, S., Roehl, C. M., Röhling, A. N., Rousogenous, C., Schneider, M., Shiomi, K., Smale, D., Stremme, W., Strong, K., Sussmann, R., Té, Y., Uchino, O., Velazco, V. A., Vigouroux, C., Vrekoussis, M., Wang, P., Warneke, T., Wizenberg, T., Wunch, D., Yamanouchi, S., Yang, Y., and Zhou, M.: Validation of methane and carbon monoxide from Sentinel-5 Precursor using TCCON and NDACC-IRWG stations, Atmos. Meas. Tech., 14, 6249–6304, https://doi.org/10.5194/amt-14-6249-2021, 2021.

Steinbrecht, W., Froidevaux, L., Fuller, R., Wang, R., Anderson, J., Roth, C., Bourassa, A., Degenstein, D., Damadeo, R., Zawodny, J., Frith, S., McPeters, R., Bhartia, P., Wild, J., Long, C., Davis, S., Rosenlof, K., Sofieva, V., Walker, K., Rahpoe, N., Rozanov, A., Weber, M., Laeng, A., von Clarmann, T., Stiller, G., Kramarova, N., Godin-Beekmann, S., Leblanc, T., Querel, R., Swart, D., Boyd, I., Hocke, K., Kämpfer, N., Maillard Barras, E., Moreira, L., Nedoluha, G., Vigouroux, C., Blumenstock, T., Schneider, M., García, O., Jones, N., Mahieu, E., Smale, D., Kotkamp, M., Robinson, J., Petropavlovskikh, I., Harris, N., Hassler, B., Hubert, D., and Tummon, F.: An update on ozone profile trends for the period 2000 to 2016, Atmos. Chem. Phys., 17, 10675–10690, https://doi.org/10.5194/acp-17-10675-2017, 2017.

Strahan, S. E., Smale, D., Douglass, A. R., Blumenstock, T., Hannigan, J. W., Hase, F., Jones, N., Mahieu, E., Notholt, J., Oman, L. D., Ortega, I., Palm, M., Prignon, M., Robinson, J., Schneider, M., Sussmann, R., and Velazco, V.: Observed hemispheric asymmetry in stratospheric transport trends from 1994 to 2018, Geophys. Res. Lett., 47, e2020GL088567, https://doi.org/10.1029/2020GL088567, 2020.

Tu, Q., Hase, F., Blumenstock, T., Schneider, M., Schneider, A., Kivi, R., Heikkinen, P., Ertl, B., Diekmann, C., Khosrawi, F., Sommer, M., Borsdorff, T., and Raffalski, U.: Intercomparison of arctic XH_2O observations from three ground-based Fourier transform infrared networks and application for satellite validation, Atmos. Meas. Tech., 14, 1993–2011, https://doi.org/10.5194/amt-14-1993-2021, 2021.

Viatte, C., Schneider, M., Redondas, A., Hase, F., Eremenko, M., Chelin, P., Flaud, J.-M., Blumenstock, T., and Orphal, J.: Comparison of ground-based FTIR and Brewer O_3 total column with data from two different IASI algorithms and from OMI and GOME-2 satellite instruments, Atmos. Meas. Tech., 4, 535–546, https://doi.org/10.5194/amt-4-535-2011, 2011.

Vigouroux, C., Bauer Aquino, C. A., Bauwens, M., Becker, C., Blumenstock, T., De Mazière, M., García, O., Grutter,

M., Guarin, C., Hannigan, J., Hase, F., Jones, N., Kivi, R., Koshelev, D., Langerock, B., Lutsch, E., Makarova, M., Metzger, J.-M., Müller, J.-F., Notholt, J., Ortega, I., Palm, M., Paton-Walsh, C., Poberovskii, A., Rettinger, M., Robinson, J., Smale, D., Stavrakou, T., Stremme, W., Strong, K., Sussmann, R., Té, Y., and Toon, G.: NDACC harmonized formaldehyde time series from 21 FTIR stations covering a wide range of column abundances, Atmos. Meas. Tech., 11, 5049–5073, https://doi.org/10.5194/amt-11-5049-2018, 2018.

Vigouroux, C., Langerock, B., Bauer Aquino, C. A., Blumenstock, T., Cheng, Z., De Mazière, M., De Smedt, I., Grutter, M., Hannigan, J. W., Jones, N., Kivi, R., Loyola, D., Lutsch, E., Mahieu, E., Makarova, M., Metzger, J.-M., Morino, I., Murata, I., Nagahama, T., Notholt, J., Ortega, I., Palm, M., Pinardi, G., Röhling, A., Smale, D., Stremme, W., Strong, K., Sussmann, R., Té, Y., van Roozendael, M., Wang, P., and Winkler, H.: TROPOMI–Sentinel-5 Precursor formaldehyde validation using an extensive network of ground-based Fourier-transform infrared stations, Atmos. Meas. Tech., 13, 3751–3767, https://doi.org/10.5194/amt-13-3751-2020, 2020.

Wang, Z., Deutscher, N. M., Warneke, T., Notholt, J., Dils, B., Griffith, D. W. T., Schmidt, M., Ramonet, M., and Gerbig, C.: Retrieval of tropospheric column-averaged CH_4 mole fraction by solar absorption FTIR-spectrometry using N_2O as a proxy, Atmos. Meas. Tech., 7, 3295–3305, https://doi.org/10.5194/amt-7-3295-2014, 2014.

WDCGG: WMO-GAW programme, available at: https://gaw.kishou.go.jp/, last access: 1 April 2021.

Weaver, D., Strong, K., Schneider, M., Deutscher, N., Blumenstock, T., Robinson, J., Notholt, J., Sherlock, V., Griffith, D., Barthlott, S., García, O., Palm, M., Jones, N., Hase, F., Kivi, R., González, Y., Sepúlveda, E., Gisi, M., Warneke, T., Dohe, S., Kohlhepp, R., Wiegele, A., Christner, E., Lejeune, B., and Demoulin, P.: Intercomparison of MUSICA and TCCON water vapour products, in: AGU Fall Meeting, San Francisco, USA, 2014.

Weaver, D., Strong, K., Schneider, M., Rowe, P. M., Sioris, C., Walker, K. A., Mariani, Z., Uttal, T., McElroy, C. T., Vömel, H., Spassiani, A., and Drummond, J. R.: Intercomparison of atmospheric water vapour measurements at a Canadian High Arctic site, Atmos. Meas. Tech., 10, 2851–2880, https://doi.org/10.5194/amt-10-2851-2017, 2017.

WMO: Quality assurance and quality control for ozonesonde measurements in GAW, World Meteorological Organization (WMO)-Report No. 201, Tech. rep., edited by: Smit, H. G. J. and the Panel for the Assessment of Standard Operating Procedures for Ozonesondes (ASOPOS), World Meteorological Organization, Geneva, Switzerland, 2014.

WMO: Scientific Assessment of Ozone Depletion: 2018, Global Ozone Research and Monitoring Project – Report No. 58, Tech. rep., World Meteorological Organization, Geneva, Switzerland, 2018.

Wunch, D., Toon, G. C., Blavier, J.-F. L., Washenfelder, R. A., Notholt, J., Connor, B. J., Griffith, D. W. T., Sherlock, V., and Wennberg, P. O.: The total carbon column observing network, Philos. T. R. Soc. A, 369, 2087–2112, https://doi.org/10.1098/rsta.2010.0240, 2011.

Wunch, D., Toon, G. C., Sherlock, V., Deutscher, N. M., Liu, X., Feist, D. G., and Wennberg, P. O.: The Total Carbon Column Observing Network's GGG2014 Data Version, TCCON Data Archive [data set] (https://tccondata.org/, last access: 1 April 2021), https://doi.org/10.14291/TCCON.GGG2014.DOCUMENTATION.R0, 2015.

Yela, M., Gil-Ojeda, M., Navarro-Comas, M., Gonzalez-Bartolomé, D., Puentedura, O., Funke, B., Iglesias, J., Rodríguez, S., García, O., Ochoa, H., and Deferrari, G.: Hemispheric asymmetry in stratospheric NO2 trends, Atmos. Chem. Phys., 17, 13373–13389, https://doi.org/10.5194/acp-17-13373-2017, 2017.

Zhou, M., Langerock, B., Wells, K. C., Millet, D. B., Vigouroux, C., Sha, M. K., Hermans, C., Metzger, J.-M., Kivi, R., Heikkinen, P., Smale, D., Pollard, D. F., Jones, N., Deutscher, N. M., Blumenstock, T., Schneider, M., Palm, M., Notholt, J., Hannigan, J. W., and De Mazière, M.: An intercomparison of total column-averaged nitrous oxide between ground-based FTIR TCCON and NDACC measurements at seven sites and comparisons with the GEOS-Chem model, Atmos. Meas. Tech., 12, 1393–1408, https://doi.org/10.5194/amt-12-1393-2019, 2019.